GeoExpert ag

swiss*nuclear*: PEGASOS Refinement Project:
SP2 – Ground Motion Characterization

Contract no. PMT-VT-1032

Seismic Shear Wave Velocity Determination and Hybrid Seismic Survey at the SED-Station MUO (Morschach, SZ)

Date of Field Data Acquisition 18th June 2009

Report

Client

swiss*nuclear*
Project PRP
Frohburgstrasse 17
4601 Olten

Contractor

GeoExpert ag
Seismic Prospecting
Ifangstrasse 12b
P.O. Box 451
8603 Schwerzenbach

8603 Schwerzenbach, 13th July 2009

INDEX

1 INTRODUCTION

1.1 Survey objectives

The seismic survey's main task is to provide information about the distribution function of the shear wave velocities in the depth interval of the uppermost 30 m along a 100 m long seismic profile.

Additionally, the following objectives are to be met:

- the mapping of the topography of the rock face, i.e. the thickness of the Quaternary deposits;
- the determination of the thickness of the weathered zone and its degree of decompaction at the bedrock surface;
- a general view of geological structures.

1.2 The choice of the appropriate surveying methods

Several methods are available for deriving the s-wave velocity distribution in the subsurface at any given position:

- in-situ measurement by down-hole or crosshole seismic surveying;
- shear-wave refraction tomography profiling;
- dispersion analysis of surface waves (MASW; **M**ultiple channel **A**nalysis of **S**urface **W**aves)

The surveys are to be carried out at, or as close as possible near some 20 SED earth quake monitoring stations in Switzerland. Ideally, the surveys are to be conducted on two orthogonal profiles in order to derive at their point of intersection a robust 1D s-wave velocity distribution function by correlation. To this end, the methods of MASW and shear-wave refraction tomography profiling are to be combined.

The results are to include the following fundamental parameters $v_{s,5}$, $v_{s,10}$, $v_{s,20}$, $v_{s,30}$, $v_{s,40}$, $v_{s,50}$, $v_{s,100}$ are to be calculated, also an error estimation of all values.

The data acquired for the MASW method are to be subjected to complementary **p-wave hybrid seismic data processing** in order to image the geological structures.

2 FIELD DATA ACQUISITION PARTICULARS

2.1 Time Schedule

Date	*Time*	*Activities / remarks*
18.06.2009	1030	arrival at site
	1030 - 1130	site investigation
	1130 - 1210	lay-out of spread profile 1 (p-wave and s-wave)
	1210 - 1245	data acquisition of spread profile 1 (p-wave)
	1305 - 1345	data acquisition of spread profile 1 (s-wave)
	1345 - 1445	lay-out of spread profile 2 (p-wave and s-wave)
	1445 - 1600	data acquisition of spread profile 2 (s-wave)
	1615 - 1640	data acquisition of spread profile 2 (s-wave)
	1640 - 1700	removal of the seismic measuring system
	1700	leaving from site

2.2 Summary of Data Acquisition Parameters

Compressional Wave Data Acquisition

# of active channels	96
geophone type	4.5 Hz natural frequency, vertical velocimeter
receiver station spacing	1.0 m
# of geophones/station	1
source point spacing	2.0 m to 3.0 m
source type	vertical hammer (8 kg) striking on a horizontal metal plate
sampling rate	500 µs
recording time	2048 ms
field filters	0.5 Hz LC, anti-alias
# of field records	48 (line 09SN_11MUO-P1) and 41 (line 09SN_11MUO-P2)

Shear Wave Data Acquisition

# of active channels	48
geophone type	10 Hz natural frequency, horizontal velocimeter
receiver station spacing	2.0 m
# of geophones/station	1
source point spacing	4.0 m to 6.0 m
source type	horizontal hammer (8 kg) striking horizontally at a metal-plated wooden beam anchored to the ground by means of 20 cm long spikes
sampling rate	500 µs
recording time	512 ms
field filters	2 Hz LC, anti-alias
# of field records	51 (line 09SN_11MUO-S1) and 48 (line 09SN_11MUO-S2)

Fig. 2.1:S-wave data acquisition at profile 09SN_11MUO-S1.

2.3 Composition of Seismic Field Crew

Personnel

Jochen Fiseli	Dipl.-Geol., University of Freiburg i. Br., geologist, party chief
Kieron Lynch	assistant, spread lay-out and activation of seismic source
Fabian Isler	assistant, spread lay-out and activation of seismic source
Volker Fink	assistant, spread lay-out and activation of seismic source

Equipment

96	vertical geophones 4.5 Hz
48	horizontal geophones 12 Hz
6	seismic cables
1	seismic acquisition system Summit Compact, 96 channels
1	laptop computer for data acquisition
3	walkie-talkies
1	hammer 8 kg
1	steel plate
1	metal-plated wooden beam
1	van (FIAT Ducato 4x4)

2.4 Location

The seismic monitoring station MUO (municipiality of Morschach, canton of Schwyz, Central Switzerland) is situated on the top of a ridge of a massive formation of Lower Cretaceous limestones.

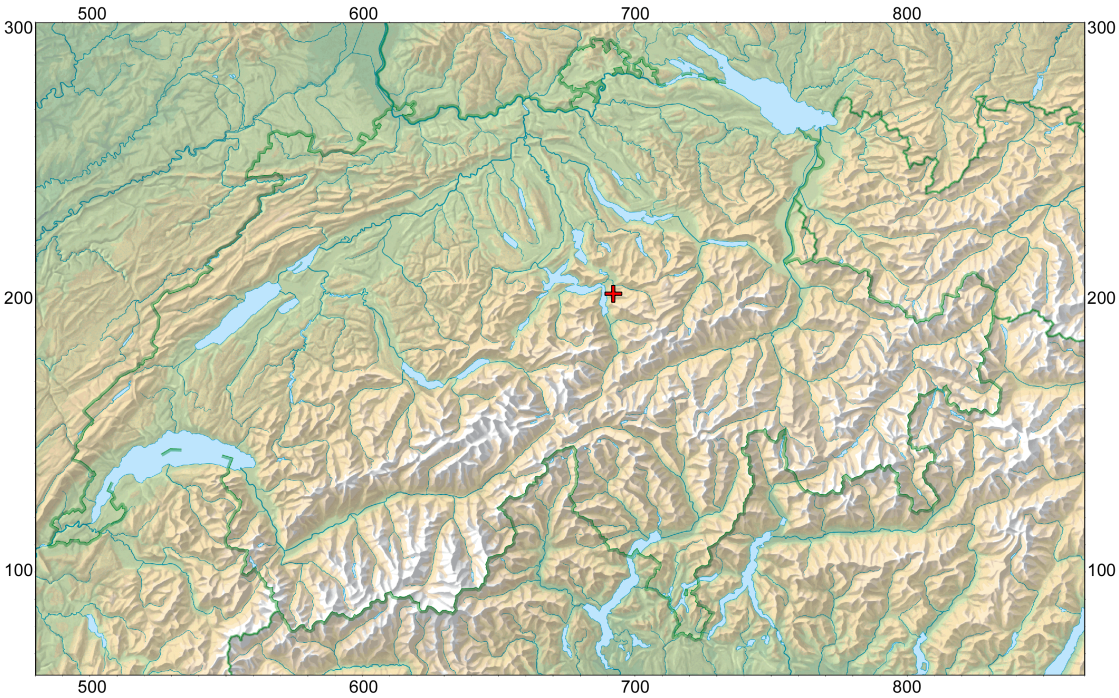

Fig. 2.2: The red cross marked seismic monitoring station MUO (Morschach, SZ) is located in Lower Cretaceous sediments. (map: geodata @ swisstopo).

2.5 Recording Conditions and Line Setup

Warm temperatures prevailed throughout the field data recording period.

In general, the data quality obtained at MUO is to be rated as fair.

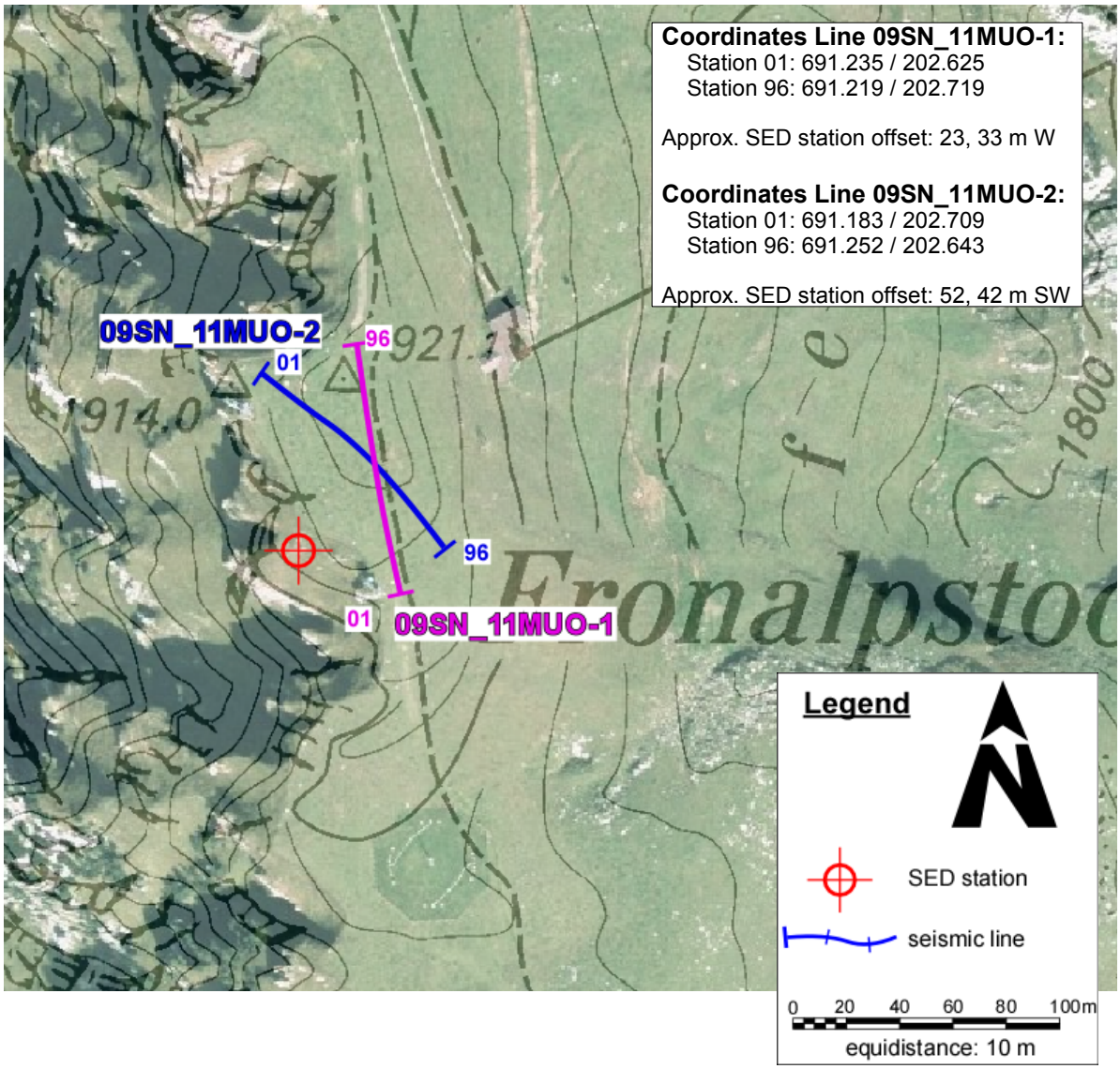

Fig. 2.3: Situation map with the trace of seismic profile 09SN_11MUO-1 and -2. (background map: © 2009 UD SZ).

3 SEISMIC DATA PROCESSING AND IMAGING OF THE RESULTS

3.1 General Remarks

- For the shear and compressional wave refraction seismic evaluation the package **RAYFRACT** by Intelligent Resources Ltd., Vancouver CAN, was used. The system features the technique of diving wave tomography (www.rayfract.com).
- The system **SPW** (**S**eismic **P**rocessing **W**orkshop) of Parallel Geoscience Corporation, Austin US-TX, was used for reflection seismic data processing (www.parallelgeo.com).
- Data processing of surface waves (MASW processing) was conducted with the software package **SurfSeis** V2.0 of Kansas Geological Survey in Lawrence US-KS.

A detailed description of the various surveying methods will be included in the general summary report.

3.2 Shear Wave Refraction Tomography

3.2.1 Reformatting and field geometry assignment

After reformatting the field data into the Rayfract format the field geometry is applied.

3.2.2 First break time picking

At each shot position, two seismic records were acquired in both activation directions. These two records are displayed superimposed with different colors on each other in Fig 3.2a together with the manually determined first arrival time picks.

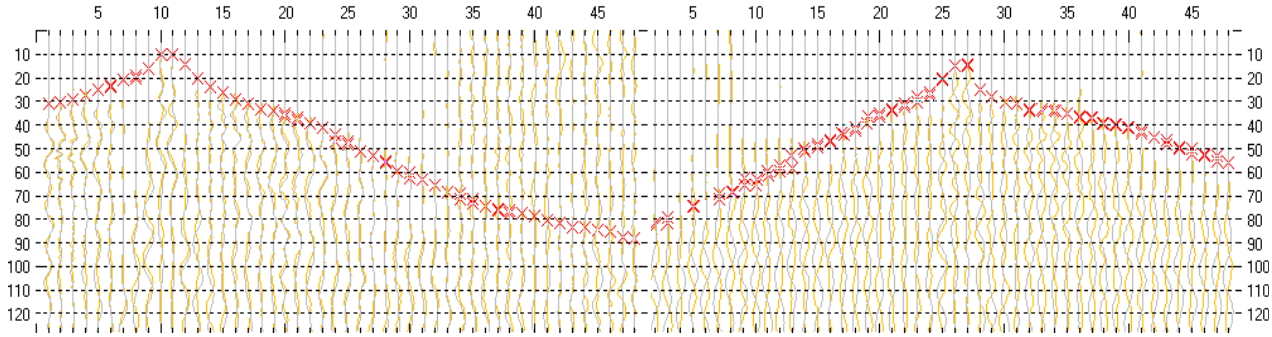

*Fig. 3.2a: High quality dual field record of line 09SN_11MUO-S1 (left) and -S2 (right).showing at each station the s-wave traces with opposing polarities in different colors. The manually picked s-wave refraction arrivals at each station are marked with an **x**. The station spacing is 2 m, profile station number 00 = profile meter 0; profile station number 48 = profile meter 96.*

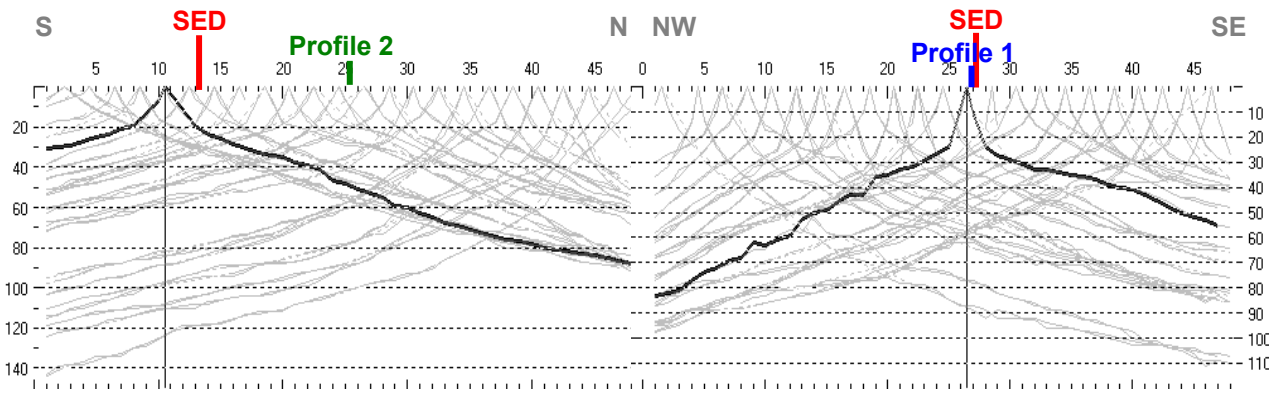

Fig. 3.2b: Curves of s-wave first break time picks of line 09SN_11MUO-S1 (left) and -S2 (right).

3.2.3 Analytical Determination of Refraction Velocities

An initial 1D-velocity function (averaged 1D velocity-depth profiles derived by the Delta-t-V method, see Tab. 3.2a) is determined in the 3-dimensional time-offset-CMP-domain of all first break arrival time curves in the 3-dimensional time-offset-CMP-domain (see. Fig. 3.2c).

Depth [m]	Vs [m/s]
0.0	198
0.3	240
0.9	323
1.2	357
1.9	439
2.8	551
4.0	702
5.8	861
8.2	1021
11.4	1088
15.7	1336
21.9	1703
30.1	2022
41.4	2450
58.2	3785

Depth [m]	Vs [m/s]
0.0	152
0.4	190
0.7	252
1.2	292
1.8	339
2.7	444
3.7	596
5.3	867
7.3	1171
10.1	1412
13.7	1457
18.8	1637
25.6	1913
34.6	2148
46.9	2364

Tab. 3.2a: Initial 1D s-wave velocity function derived from real data of line 09SN_11MUO-S1 (mean values of all derivations) and of line 09SN_11MUO-S2 (mean values of all derivations).

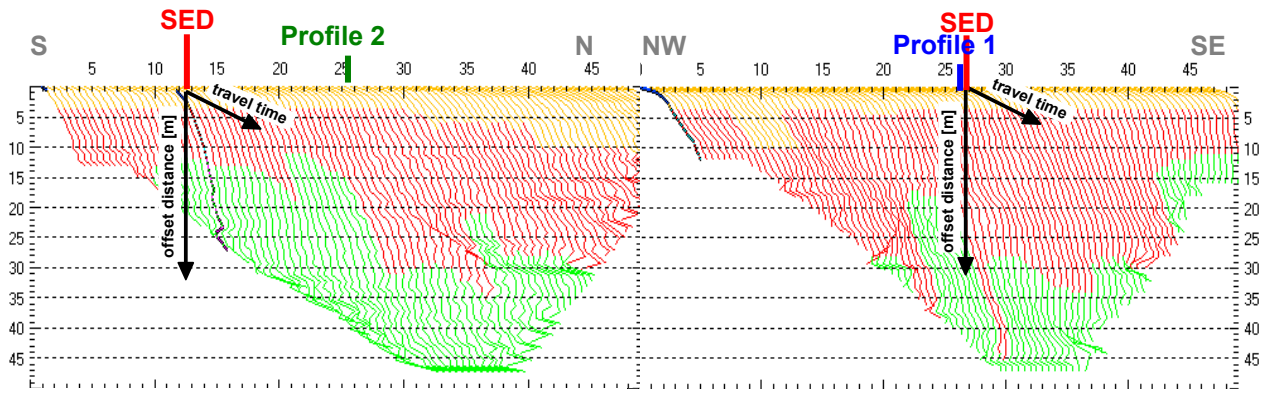

Fig. 3.2c: 3-dimensional distance-travel time diagrams of line 09SN_11MUO-S1 (left) and -S2 (right) at the mid-points between source points and receiver stations are instrumental when using the analytical CMP derivation of the initial velocity field.
The horizontal axes are the along the CMP positions and the travel time respectively, the vertical axis denotes the offset distance between source and receiver positions. The colors represent different velocity layers. The station spacing is 2 m, profile station number 00 = profile meter 0; profile station number 48 = profile meter 96. The colors represent different velocity layers.

3.2.4 Tomographic inversion of the velocity gradient field by iterative modeling

The velocity field is iteratively refined by the subsequent Wavepath Eikonal Traveltime (WET) tomographic inversion process. The inversion results are portrayed in Fig. 3.2d as a gridded velocity contour section and in Fig. 3.2e as a ray path density section.

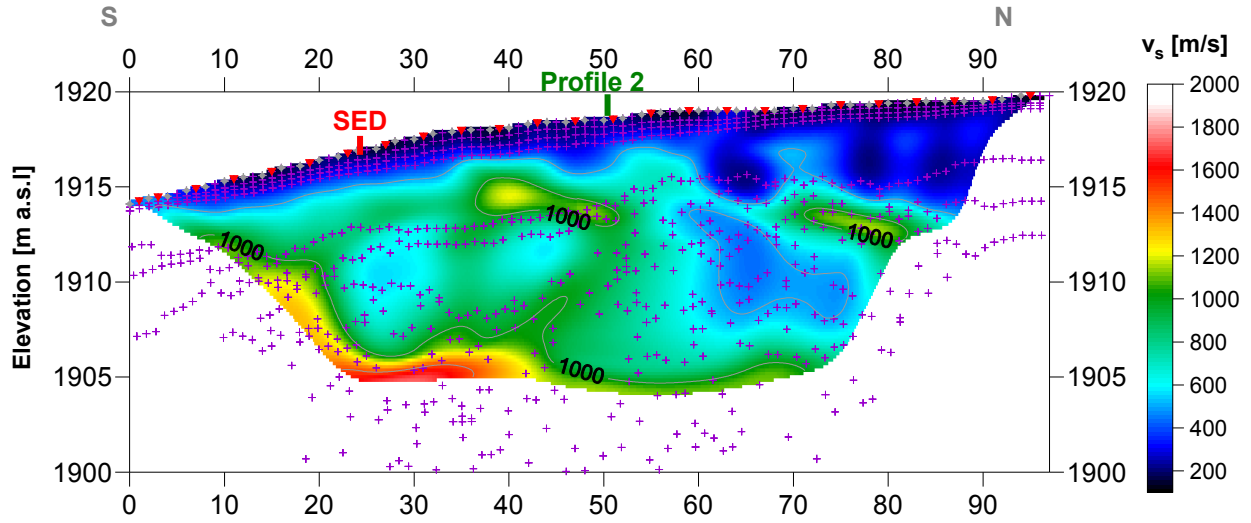

Fig. 3.2d: Shear wave velocity field of the line 09SN_11MUO-S1. Red/white colors denote solid rock, blue/black colors point to unconsolidated sediments and soil.
Vertical axis: elevation [m a.s.l]; horizontal axis: profile meter; color encoded scale: v_s [m/s]; vertical exaggeration: 2:1; gray diamonds: receiver positions; red triangles: source positions; magenta crosses: positions of determined velocity values. The station spacing is 2 m, profile meter 0 = profile station number 00, profile meter 96 = profile station number 48.

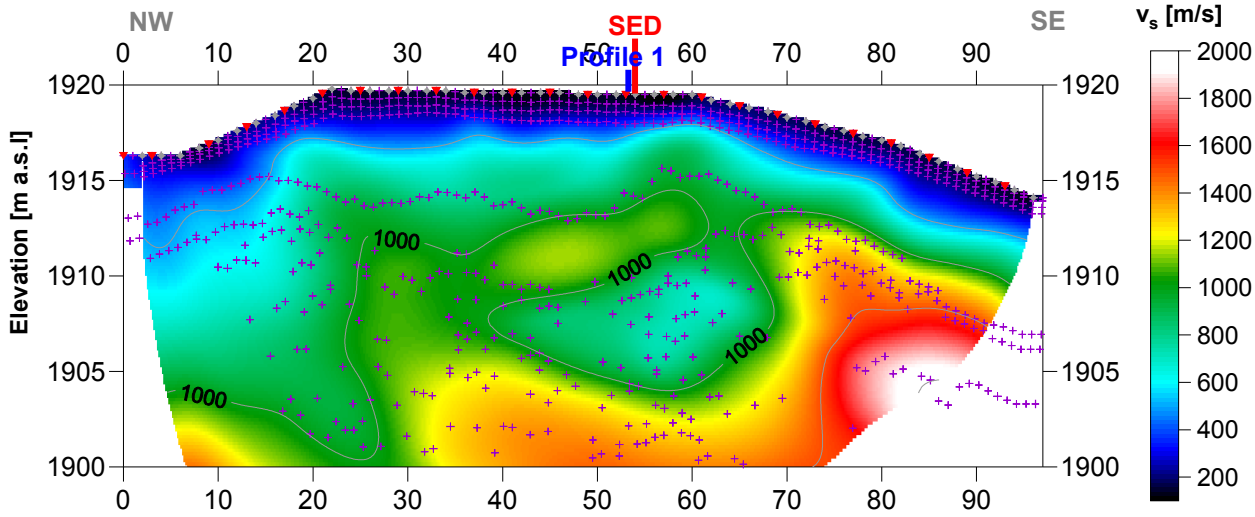

Fig. 3.2e: Shear wave velocity field of the line 09SN_11MUO-S2. Red/white colors denote solid rock, blue/black colors point to unconsolidated sediments and soil.
Vertical axis: elevation [m a.s.l]; horizontal axis: profile meter; color encoded scale: v_s [m/s]; vertical exaggeration: 2:1; gray diamonds: receiver positions; red triangles: source positions; magenta crosses: positions of determined velocity values. The station spacing is 2 m, profile meter 0 = profile station number 00, profile meter 96 = profile station number 48.

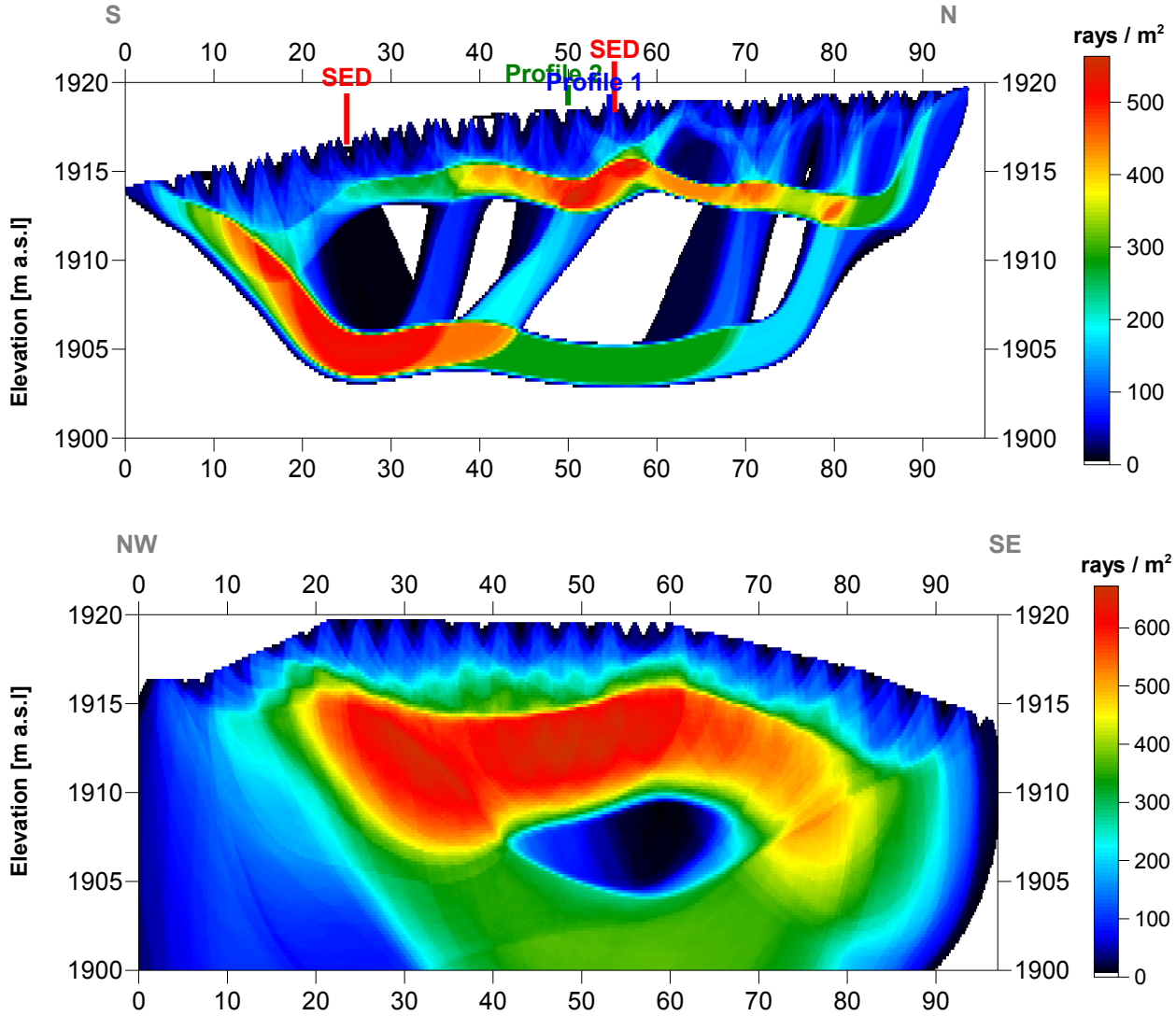

Fig. 3.2f: Shear wave ray path density along the seismic line 09SN_11MUO-S1 (top) and -S2 (bottom). Red/white colors indicate high velocity contrasts (usually at the bedrock surface), blue/black colors denote low coverage areas. Vertical axis: elevation [m a.s.l]; horizontal axis: profile meter; color encoded scale: ray paths per m²; vertical exaggeration: 2:1. The station spacing is 2 m, profile meter 0 = profile station 00, profile meter 96 = profile station 48.

Depth [m]	Vs [m/s]
0.0	198
1.0	337
2.1	514
3.1	634
4.2	708
5.2	768
6.3	773
7.3	724
8.4	723
9.4	757
10.5	797
11.5	904
12.6	1016
13.6	991
14.7	1109

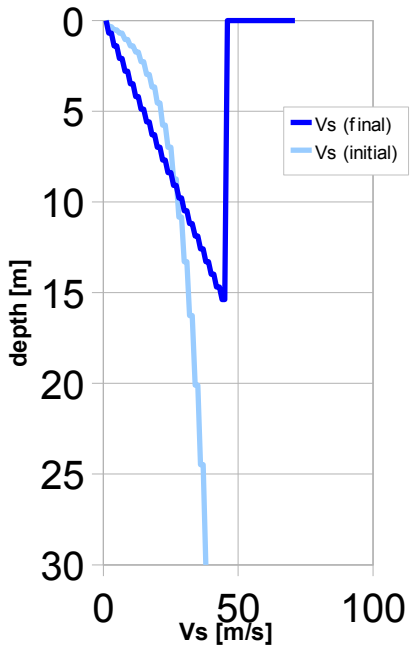

Tab. 3.2b: Final 1D s-wave velocity model derived from real data of line 09SN_11MUO-S1 (horizontal average of all values). The calculated values of the initial 1D s-wave velocity model are given in Tab. 3.2a.

Depth [m]	Vs [m/s]
0.0	162
1.8	415
3.6	694
5.3	894
7.1	1031
8.9	1065
10.7	1047
12.4	1066
14.2	1111
16.0	1200
17.6	1277
19.4	1332
21.1	1372
22.9	1407
24.7	1370
26.5	1415
28.2	1497

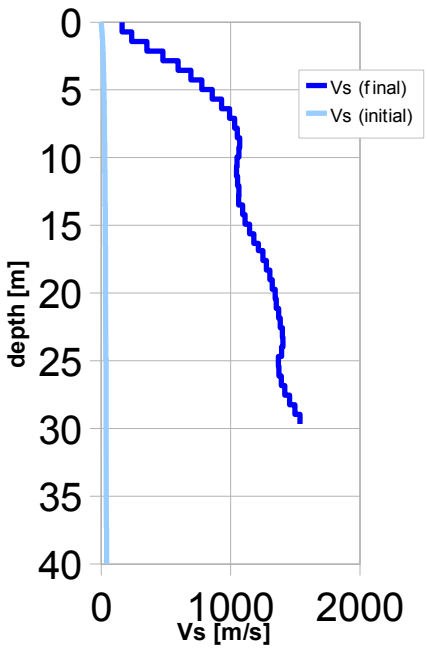

Tab. 3.2c: Final 1D s-wave velocity model derived from real data of line 09SN_11MUO-S2 (horizontal average of all values) The calculated values of the initial 1D s-wave velocity model are given in Tab. 3.2a.

3.3 MASW Processing

3.3.1 Reformatting and field geometry assignment

The data preparation steps for the dispersion analysis include

- the assignment of the field acquisition geometry
- the selection of suitable offset ranges (=arrays) between 10 m and 50 m for dispersion, and the splitting of the field records in forward and reverse shooting direction data sets
- the reformatting of the data into the specific KGS format

X - - ... - - o-o-o-...-o-o-o (forward shooting or so-called PLUS direction)
respectively
o-o-o-...-o-o-o - - ... - - X (reverse shooting or so-called MINUS direction).

where **X** = shot position
o = receiver station
- = 1.0 m offset

The active array used at SED-station MUO are the receiver station in the shot offset range between 10 and 50 m.

3.3.2 Calculating the dispersion image (overtone)

The result of dispersion analysis is the color encoded acoustic energy distribution in the phase velocity - frequency plane (see Fig. 3.3a and b).

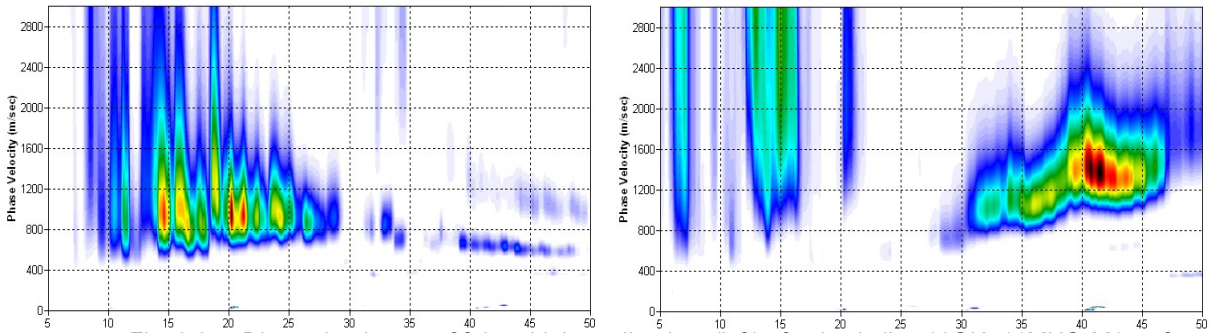

Fig. 3.3a: Dispersion image of fair to high quality data (left) of seismic line 09SN_11MUO-M1 as found on 70 % and of deficient quality data (right) of seismic line 09SN_11MUO-M2 representing about 30 % of the MASW dataset of site MUO.
Horizontal axis: frequency from 5 to 50 Hz; vertical axis: phase velocity from 0 to 3000 m/s; color code: colors from white (no energy) to blue - green - yellow - red - black point to increasing energy amplitude values.

3.3.3 Analysis of the dispersion image

In the dispersion graphs as calculated in section 3.3.2 above, the curves joining the amplitude peaks of the fundamental modes are determined either by subjective inspection or in a semi-automated manner. On datasets with poorly defined amplitude peaks or with a highly irregular alignment of the peaks, the danger of obtaining improbable or wrong results is real and can only be mitigated by the processing experience and the a-priori knowledge of the geological setting by the geophysicist responsible for the data evaluation.

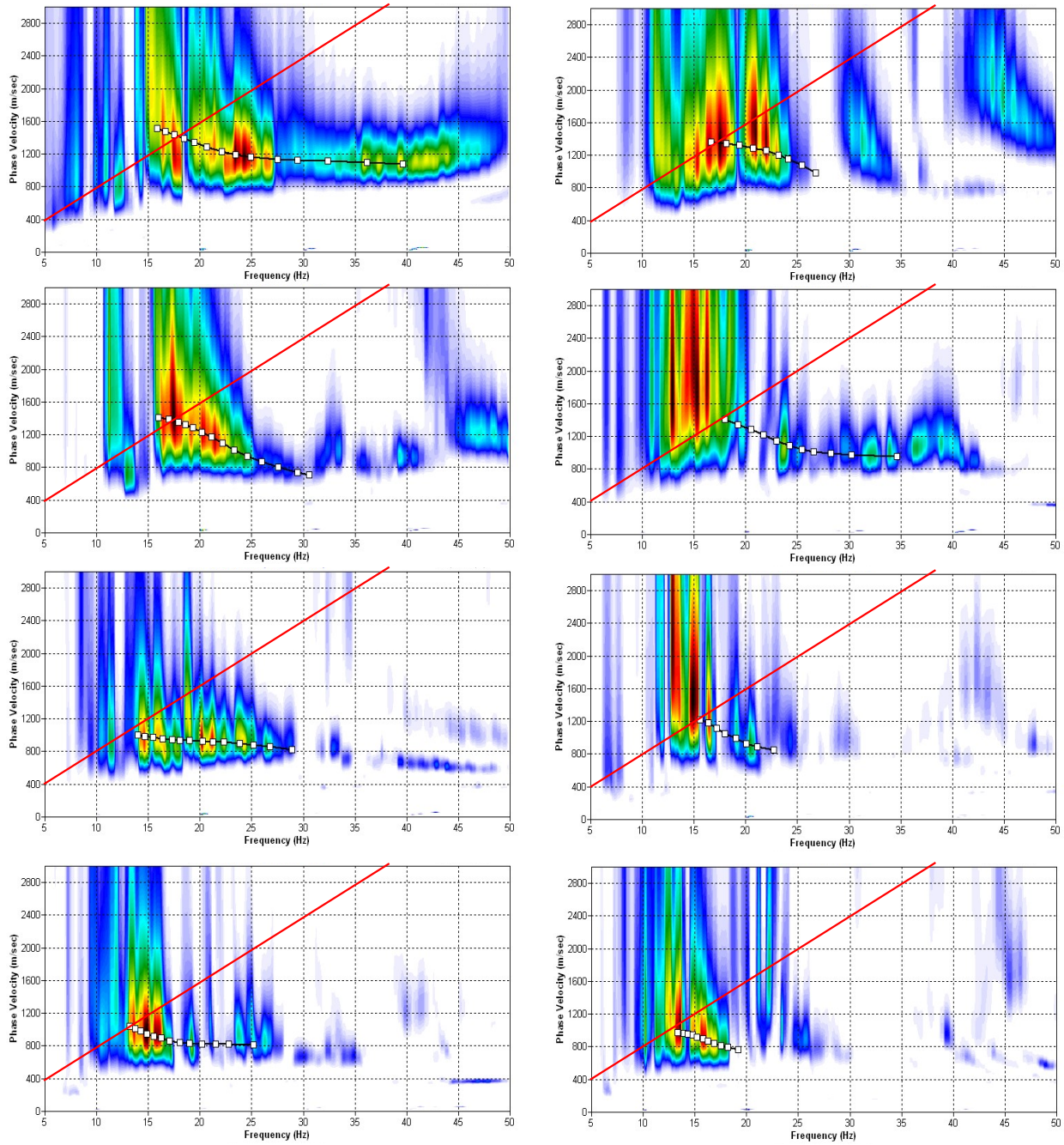

Fig. 3.3b: The manually picked dispersion images used for the derivation of the shear wave velocity section on line 09SN_11MUO-M1. The dispersion curves (squares) are determined by linking the peaks of high energy. Note that 'higher modes' may at times produce higher energy peaks than the fundamental mode required for the analysis.
dotted fine line: signal-noise ratio for the designated f-v_{ph} – value.
red line: high resolution beam-forming curve for v_{max}.
1st row: left: station 25 @ PLUS direction; right: station 21 @ MINUS direction
2nd row: left: station 41 @ PLUS direction; right: station 39 @ MINUS direction
3rd row: left: station 58 @ PLUS direction; right: station 62 @ MINUS direction
4th row: left: station 76 @ PLUS direction; right: station 76 @ MINUS direction

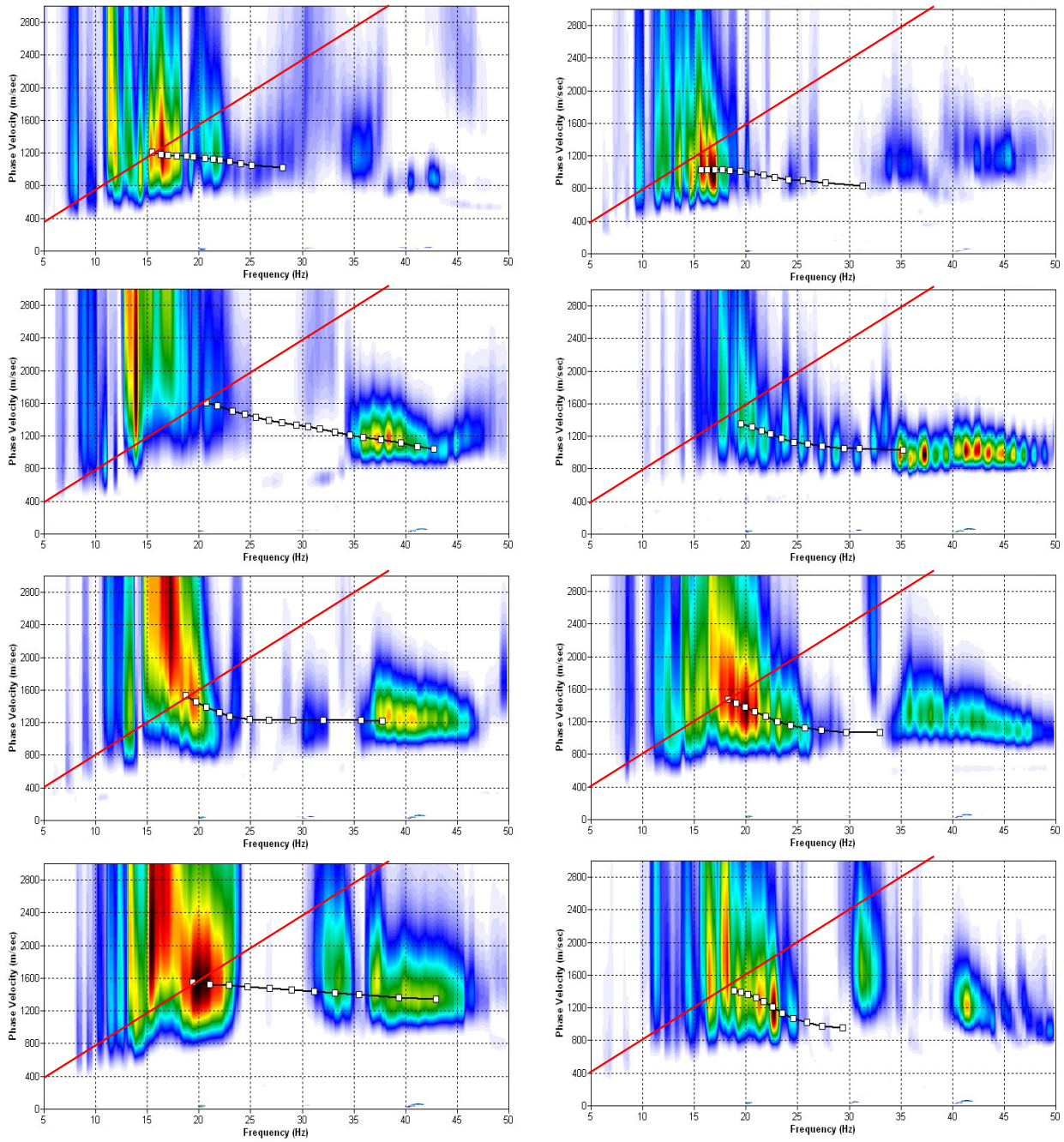

Fig. 3.3c: The manually picked dispersion images used for the derivation of the shear wave velocity section on line 09SN_11MUO-M2. The dispersion curves (squares) are determined by linking the peaks of high energy. Note that 'higher modes' may at times produce higher energy peaks than the fundamental mode required for the analysis.
dotted fine line: signal-noise ratio for the designated f-v_{ph} – value.
red line: high resolution beam-forming curve for v_{max}.
1st row: left: station 25 @ PLUS direction; right: station 21 @ MINUS direction
2nd row: left: station 46 @ PLUS direction; right: station 39 @ MINUS direction
3rd row: left: station 58 @ PLUS direction; right: station 51 @ MINUS direction
4th row: left: station 76 @ PLUS direction; right: station 66 @ MINUS direction

3.3.4 Inversion of dispersion curves resulting in a 1D shear wave velocity distribution

Inversion of the extracted dispersion curves was performed using the algorithm described by Xia et al. (1999).

The inversion process is started by setting the maximum depth (z_{max}) to be in the order of 30% of the largest wavelength for an initial model consisting of 10 layers of increasing thicknesses. For all 10 layers the Poisson's ratio is assumed to be 0.4 and the rock/soil density to be 2.0 g/cm^3. The inversion process is concluded either after twelve iterations or when the convergence condition of a RMS-error of less than 3 m/s (phase velocity) is met.

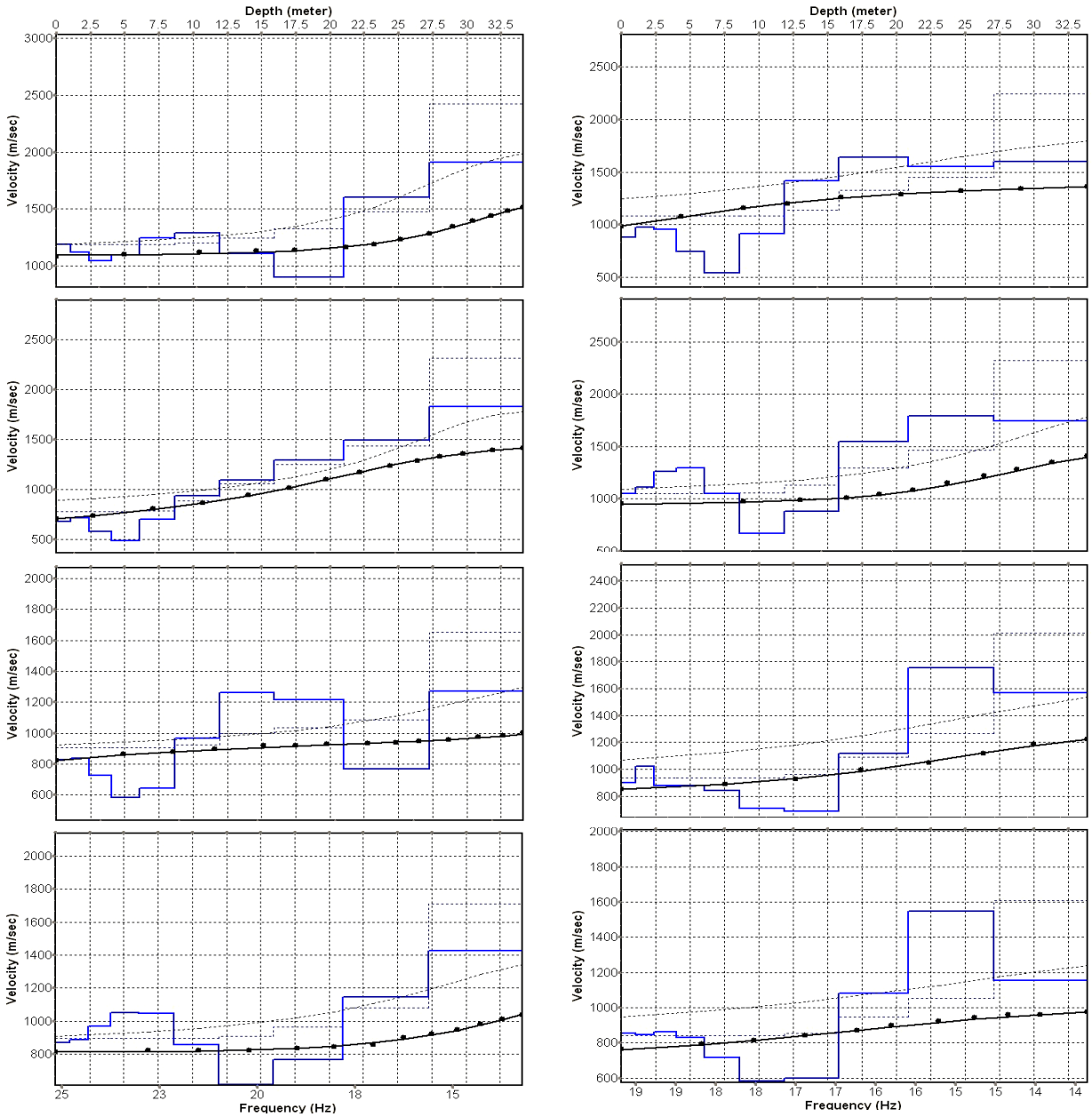

Fig. 3.3d: Inversion results of dispersion curves of dataset at line 09SN_11MUO-M1.
***brown**: Inversion of dispersion curve (dots) resp. of the modeled dispersion curve (dotted line: initial model; continuous line: end model). Horizontal axis: frequency Hz, vertical axis: v_s.*
***blue**: 10-layer-model (dotted: initial model, continuous line: final model). Horizontal axis: depth, vertical axis: phase velocity resp. v_s).*
1st row: left: station 25 @ PLUS direction; right: station 21 @ MINUS direction
2nd row: left: station 41 @ PLUS direction; right: station 39 @ MINUS direction
3rd row: left: station 58 @ PLUS direction; right: station 62 @ MINUS direction
4th row: left: station 76 @ PLUS direction; right: station 76 @ MINUS direction

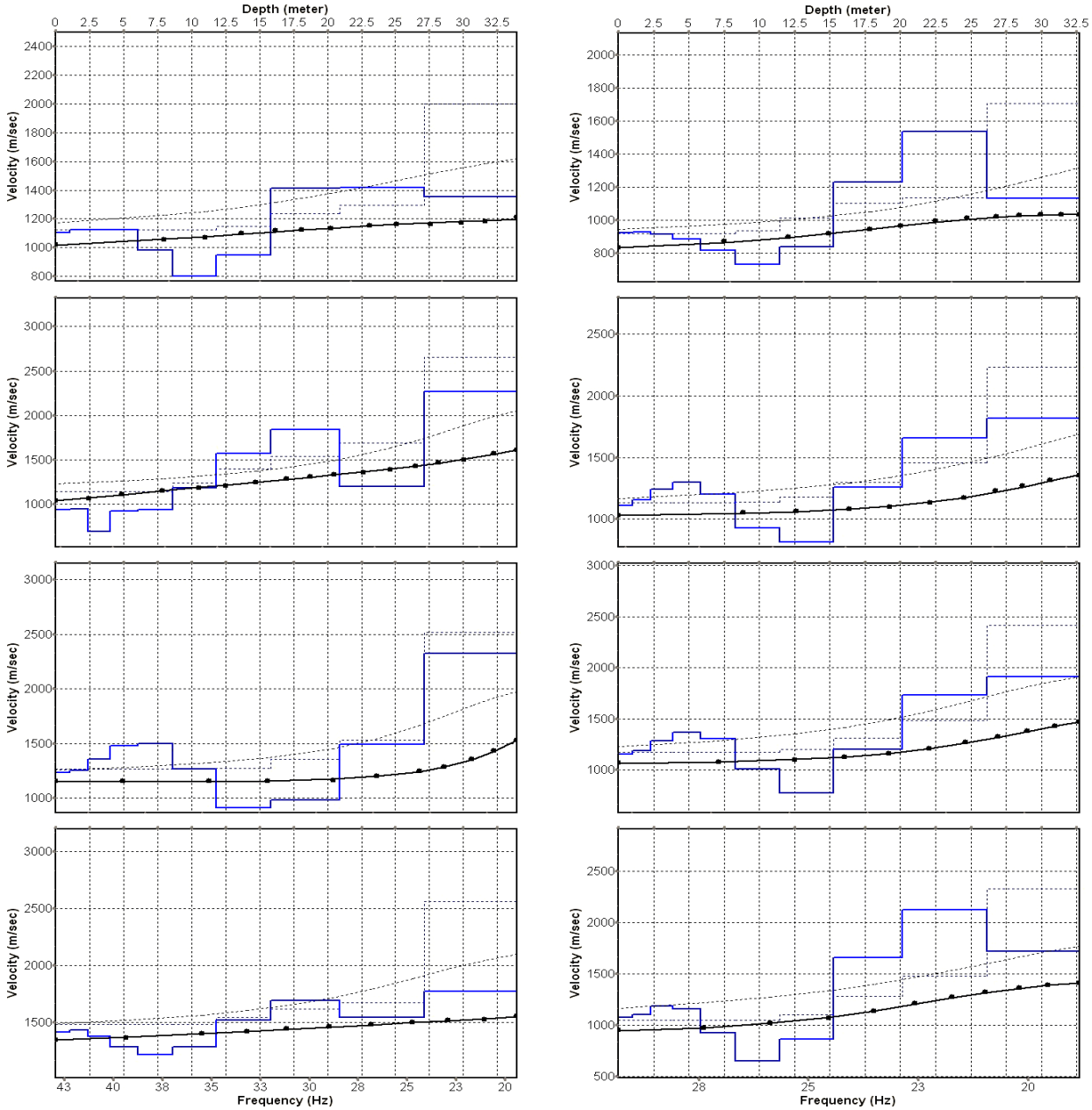

Fig. 3.3e: Inversion results of dispersion curves of dataset at line 09SN_11MUO-M2.
***brown**: Inversion of dispersion curve (dots) resp. of the modeled dispersion curve (dotted line: initial model; continuous line: end model). Horizontal axis: frequency Hz, vertical axis: v_s.*
***blue**: 10-layer-model (dotted: initial model, continuous line: final model). Horizontal axis: depth, vertical axis: phase velocity resp. v_S).*
1st row: left: station 28 @ PLUS direction; right: station 31 @ MINUS direction
2nd row: left: station 40 @ PLUS direction; right: station 41 @ MINUS direction
3rd row: left: station 49 @ PLUS direction; right: station 47 @ MINUS direction
4th row: left: station 58 @ PLUS direction; right: station 56 @ MINUS direction

Dispersion analyses of records with longer receiver arrays should – by theory – increase the investigation depth. At MUO, with both lines and both directions, MASW processing with the maximal array length of 96 m improves the results (Fig. 3.3f and 3.3g).

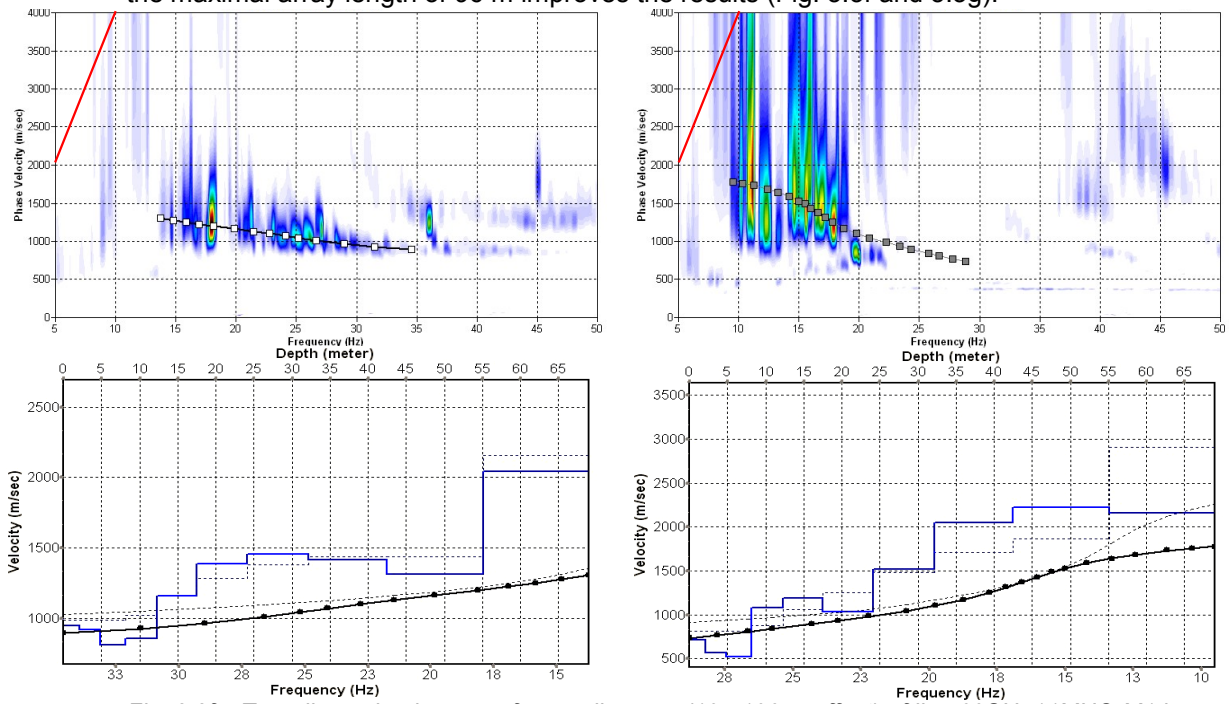

Fig. 3.3f: Top: dispersion images of over-all arrays (10...106 m offset) of line 09SN_11MUO-M1 in PLUS (left) and MINUS (right) direction; dotted fine line: signal-noise ratio for the designated f-v_{ph}-value. Red line: high resolution beam-forming curve for v_{max}.
*Below: The two respective inversion results; **brown**: inversion of dispersion curve; **blue**: 10-layer-model. Horizontal axis: depth, vertical axis: phase velocity resp. v_s.*

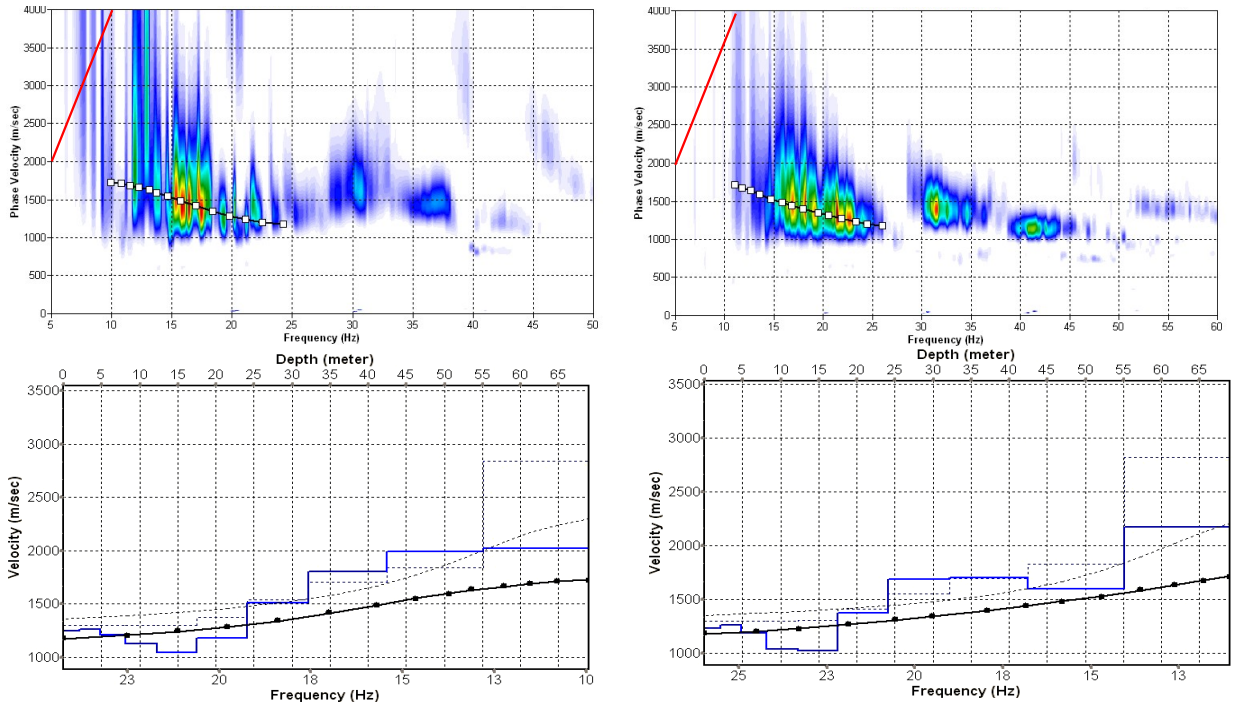

Fig. 3.3g: Top: dispersion images of over-all arrays (10...106 m offset) of line 09SN_11MUO-M2 in PLUS (left) and MINUS (right) direction; dotted fine line: signal-noise ratio for the designated f-v_{ph} – value. Red line: high resolution beam-forming curve for v_{max}.
*Below: The two respective inversion results; **brown**: inversion of dispersion curve; **blue**: 10-layer-model. Horizontal axis: depth, vertical axis: phase velocity resp. v_s.*

3.3.5 Gridding and plotting of 2D v_s-velocity field

By assembling the 1D v_s - depth functions of all stations the final 2D v_s-field is derived using a Kriging gridding procedure as portrayed in Fig. 3.3h and 3.3i below:

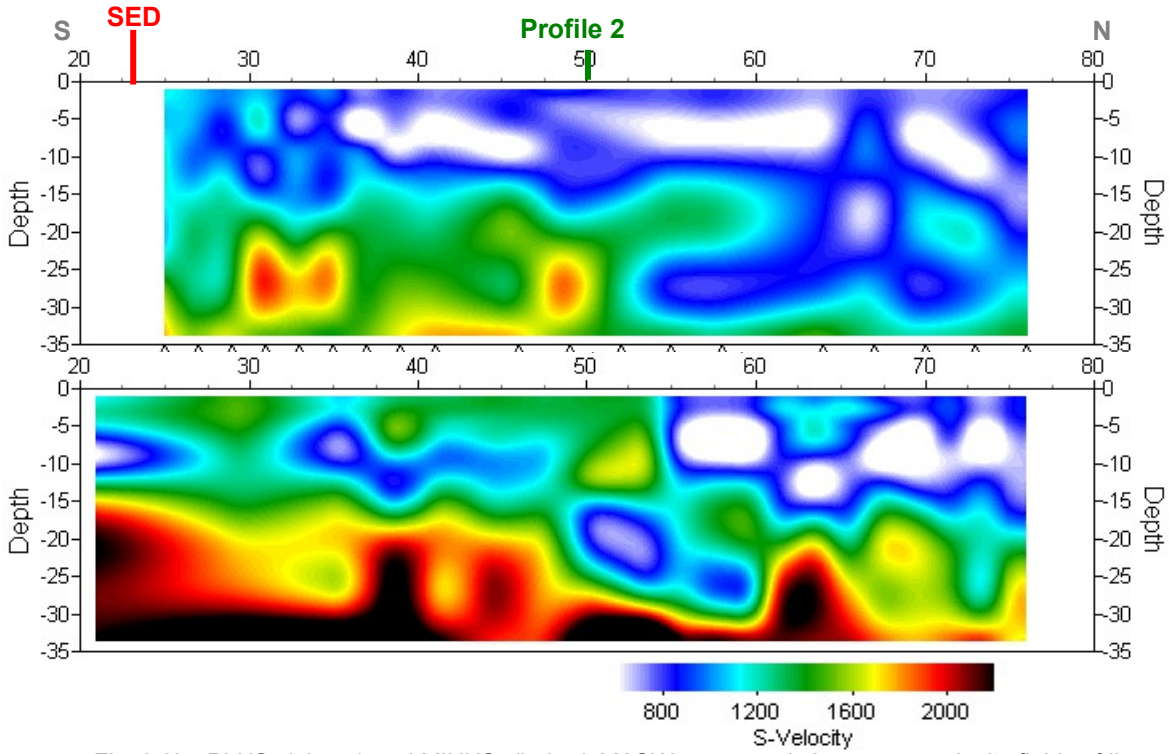

Fig. 3.3h: PLUS- (above) and MINUS- (below)-MASW-processed shear wave velocity fields of line 09SN_11MUO-M1. Station spacing is 1 m.

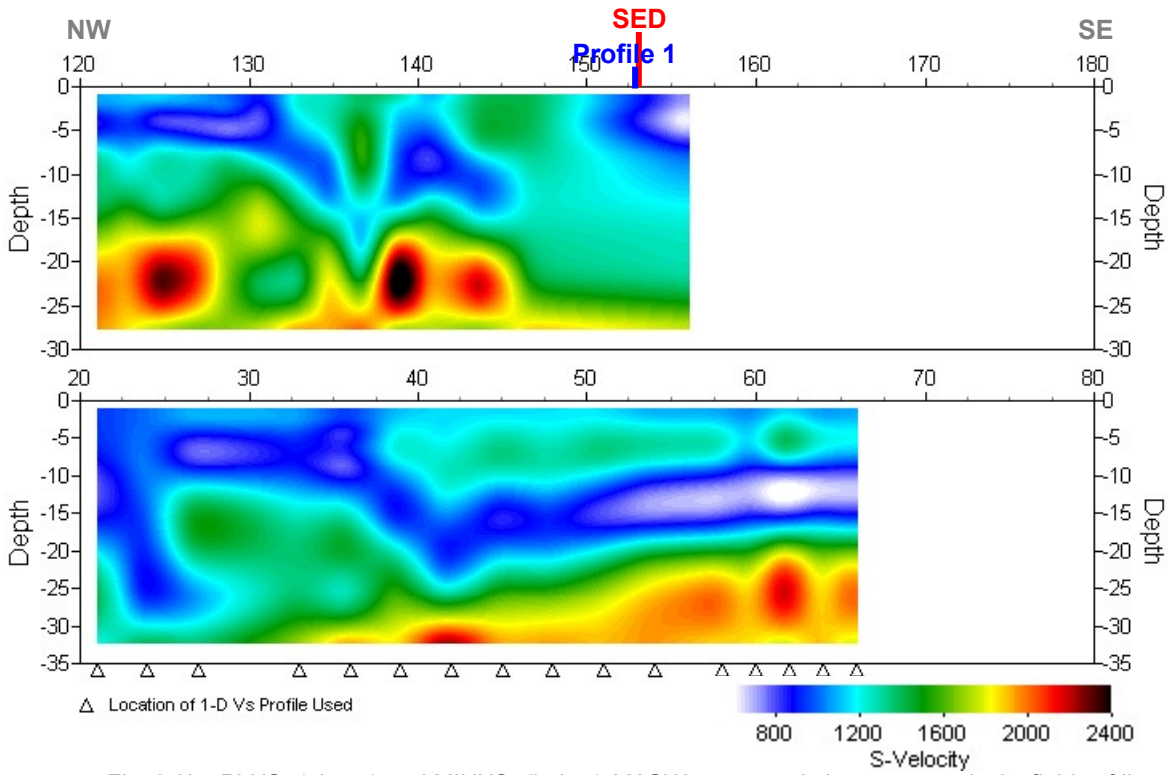

Fig. 3.3i: PLUS- (above) and MINUS- (below)-MASW-processed shear wave velocity fields of line 09SN_11MUO-M2. Station spacing is 1 m.

3.3.6 Calculation of the average shear wave velocity

In order to calculate a representative shear wave velocity-depth function of line 09SN_11MUO-M1 at the SED station, all computed 1D-v_s-depth functions are averaged (non-weighted mean values). The v_s-depth-function is shown in Tab. 3.3a.

Depth [m]	Vs+ [m/s]	Vs- [m/s]	Vs [m/s]
1.1	863	857	860
2.4	919	849	884
4.0	869	794	832
6.1	792	761	776
8.7	746	797	771
11.9	823	902	862
15.9	975	1062	1018
20.9	1165	1233	1199
27.2	1265	1310	1288
34.0	1609	1497	1553

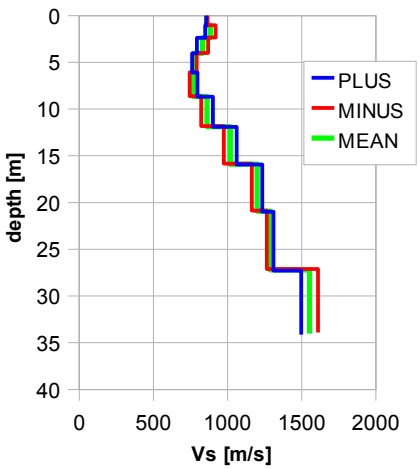

Tab. 3.3a: Averaged vs - depth function of line 09SN_11MUO-M1 at the SED station MUO. Blue line: MASW-'PLUS' processing, red line: MASW-'MINUS' processing; green line: average of PLUS- and MINUS-functions.

In order to calculate an representative shear wave velocity-depth function of line 09SN_11MUO-M2 at the SED station, all computed 1D-v_s-depth functions are averaged (non-weighted mean values). The resulting v_s-depth-function is shown in Tab. 3.3b.

Depth [m]	Vs- [m/s]	Vs+ [m/s]	Vs [m/s]
1.0	1068	1141	1105
2.3	1100	1150	1125
3.9	1133	1099	1116
6.0	1148	1085	1117
8.5	1056	1108	1082
11.6	906	1186	1046
15.6	957	1260	1109
20.5	1326	1314	1320
26.7	1620	1283	1452
33.3	1800	2024	1912

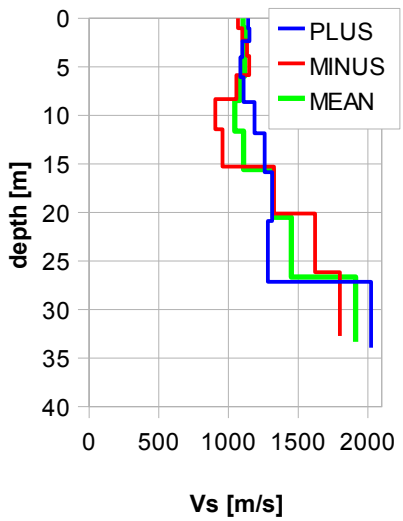

Tab. 3.3b: Averaged v_s - depth function of line 09SN_11MUO-M2 at the SED station MUO. Blue line: MASW-'PLUS' processing, red line: MASW-'MINUS' processing; green line: average of PLUS- and MINUS-functions.

The inversion of the four 100 m-array dispersion curves data (10 to 106 m offset, see Fig. 3.3f and 3.3g) are given in Tab. 3.3c. These values are complemented with the values derived of the 40 m-arrays analyses (Tab. 3.3a and 3.3b).

	100 m array							40 m array					
depth	m1+	m1-	m2+	m2-	m1	m2	m	depth	m1	depth	m2	depth	m
2.1	944	715	1247	1229	829	1238	968	1.1	860	1.0	1105	1.0	982
4.8	920	567	1262	1260	743	1261	916	2.4	884	2.3	1125	2.3	1004
8.2	810	525	1206	1184	668	1195	847	4.0	832	3.9	1116	4.0	974
12.3	855	1080	1124	1035	968	1079	1020	6.1	776	6.0	1117	6.0	947
17.6	1155	1188	1045	1024	1171	1034	1129	8.7	771	8.5	1082	8.6	927
24.1	1384	1038	1174	1371	1211	1273	1199	11.9	862	11.6	1046	11.8	954
32.2	1456	1516	1506	1688	1486	1597	1493	15.9	1018	15.6	1109	15.7	1064
42.4	1415	2049	1803	1703	1732	1753	1756	20.9	1199	20.5	1320	20.7	1260
55.2	1312	2220	1990	1598	1766	1794	1841	27.2	1288	26.7	1452	26.9	1370
69.0	2041	2161	2021	2171	2101	2096	2074	34.0	1553	33.3	1912	33.7	1733

Tab. 3.3c: v_s-depth values of the four MASW-derived dispersion curves of both seismic line 09SN_11MUO-M1 and 09SN_11MUO-M2 using 100 m-arrays. The dispersion curves are shown in Fig. 3.3f and Fig 3.3g.

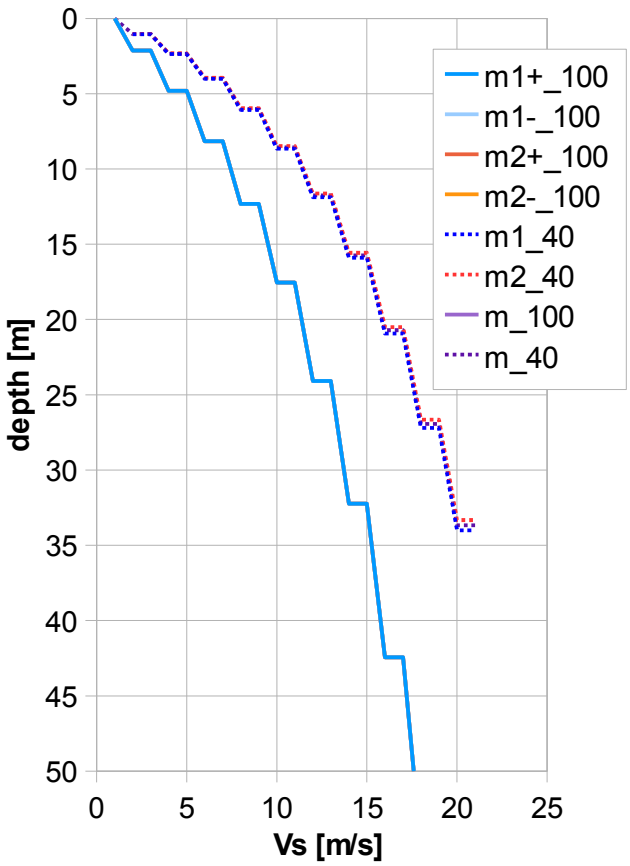

Fig. 3.3j: Comparison of the ensemble of inversion results of both lines 09SN_11MUO-M1 and -M2, either using the 40-m- and the 100-m-arrays.
blue lines: analyses of records of line 09SN_11MUO-M1
red lines: analyses of records of line 09SN_11MUO-M2
magenta line: mean of both 100-m-array records analyses in MINUS and PLUS direction.
dotted lines: v_s-values of analyses of 40-m-array records.

3.3.7 Calculation of the shear wave velocity scalars $v_{s,5}$, $v_{s,10}$, ...

The parameters $v_{s,5}$, $v_{s,10}$, $v_{s,20}$, $v_{s,30}$, $v_{s,40}$, $v_{s,50}$ represent the average shear wave velocities in the depth interval between the surface and the respective depth levels and are determined from the formula

$$v_{s,n} = \frac{\sum_{i=1}^{n} d_i}{\sum_{i=1}^{n} d_i / v_{si}}$$

with:

d_i = thickness of layer i
v_{si} = corresponding shear-wave velocity.

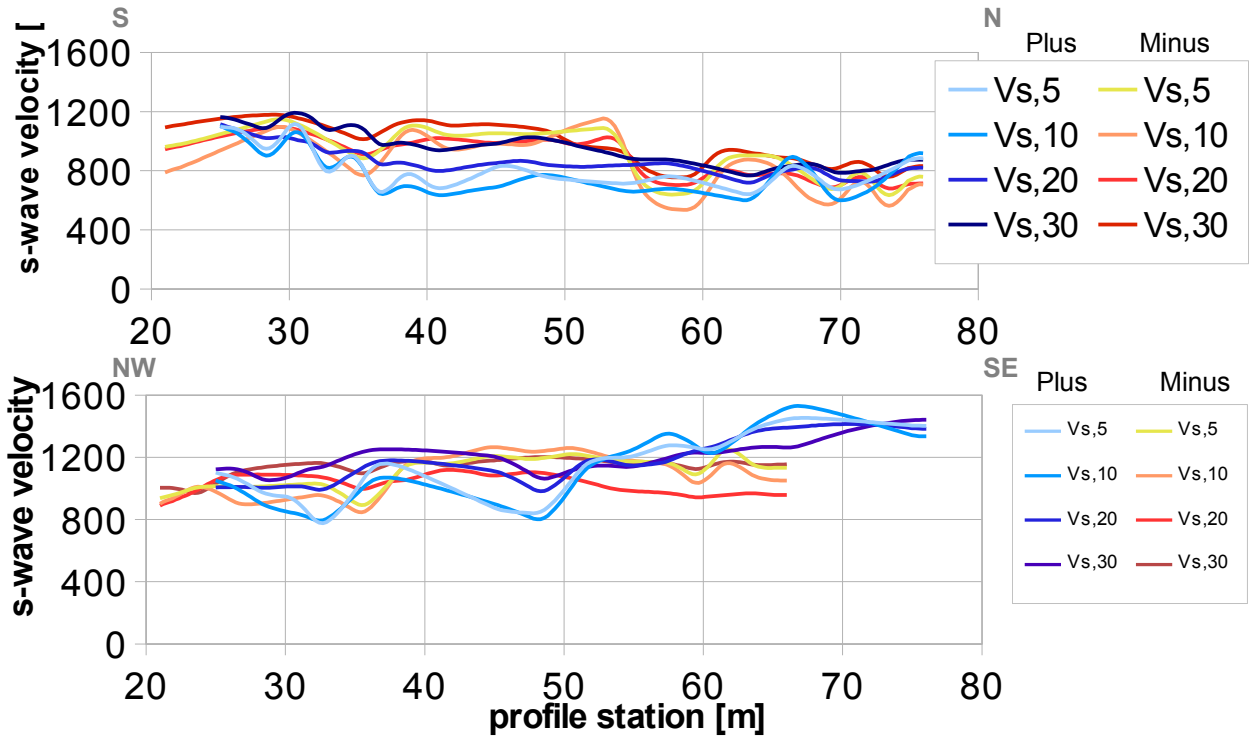

Fig. 3.3k: Graphs of the averaged $v_{s,5}$...-values along the line 09SN_11MUO-M1 (top) resp. -M2 (bottom) for the PLUS- (blue lines) and MINUS- (red lines) directions.

The average values of the s-wave velocity model $v_{s,5}$, $v_{s,10}$, $v_{s,20}$, $v_{s,30}$, $v_{s,40}$, $v_{s,50}$, $v_{s,100}$ (= average shear wave velocity from the surface to depths of 5 m, … until 40 m) on the line segment nearest to the SED station (Tab. 3.3d) are summarized below:

	Vs,5	Vs,10	Vs,20	Vs,30	Vs,40
MINUS	932	863	904	995	n/a
PLUS	792	755	851	946	n/a
MEAN	862	809	877	970	n/a

	Vs,5	Vs,10	Vs,20	Vs,30	Vs,40
MINUS	1107	1086	1032	1142	n/a
PLUS	1151	1139	1189	1216	n/a
MEAN	1129	1113	1111	1179	n/a

Tab. 3.3d: The average shear wave velocities within the depth intervals from surface down to 5 m, etc.… to 50 m, calculated for the whole line;
line 09SN_11MUO-M1 (top) and line -M2, (bottom).

3.4 Hybrid Seismic Data Processing

3.4.1 p-wave *Reflection* Seismic Processing Sequence

A) Data conditioning

A1 Reformatting and quality verification of field data
A2 Recording geometry assignment
A3 Data editing (suppression of bad / dead traces, etc.)
A4 Preliminary analysis of refraction velocities

B Filtering and deconvolution

B1 Analytical muting of refraction arrivals
B2 Amplitude recovery / amplitude equalization in time and frequency domains
B3 Predictive deconvolution parameter tests / application
B4 Determination of band limiting corner frequencies / application
B5 Optional 2-D filtering

C) Velocity analysis and stack

C1 Common Depth Point (CDP) sort
C2 Semblance velocity analysis using supergathers of 3 - 5 CDP's
C3 Optional dip move-out correction
C4 Normal Move-Out (NMO) correction and application of stretch mute
C5 Band-pass filtering
C6 CDP stack
C7 Optional coherency filtering

D) Time-depth conversion

D1 Optional spiking deconvolution
D2 Band-pass filtering
D3 Depth conversion
D4 Final display of seismic depth section with inversed polarity (non-SEG-convention)

3.4.2 The presentation of reflection seismic data

The data in a reflection seismic section are presented as an assembly of individual seismic signals at regular intervals along a seismic profile. The simplest way of representing the signals are single wiggle lines (first to the left in the illustration below). A more capturing presentation is the variable area form (second to the left). Combining these two modes results in the var-wiggle mode. Another method of data visualization is the variable density mode (second from the right).

The compressional phase of seismic signals is defined in this report as the onset of the positive amplitude excursion in black (Fig. 3.4a). Since the source signal is produced by an explosion or by an impact at the surface, the signal starts off with a compression of the ground particles. Thus the arrivals of reflection events are defined by the compressional phase.

In rare situations of velocity inversions, cases in which formation velocities are lower than in the layers above, polarity reversals of the reflected signals occur. The beginning of the reflection event would then be characterized by a dilatational phase, represented in this report as a negative amplitude excursion, i.e. in white.

The final p-wave seismic depth sections are displayed in Fig. 3.4b and 3.4c, the hybrid sections in Fig. 3.4j and -k further below.

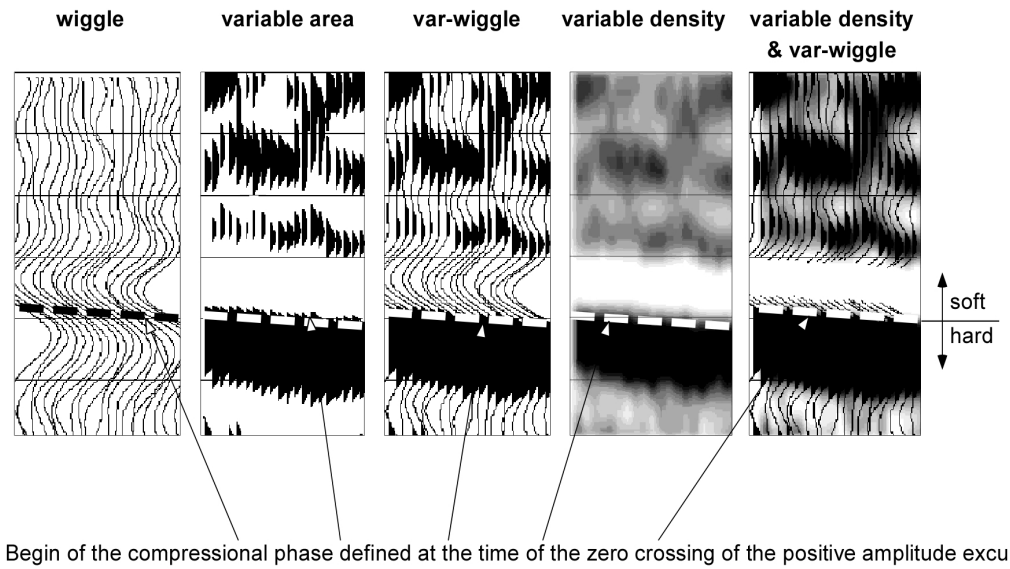

Fig. 3.4a Representation of reflection seismic data and the definition of a reflection event.

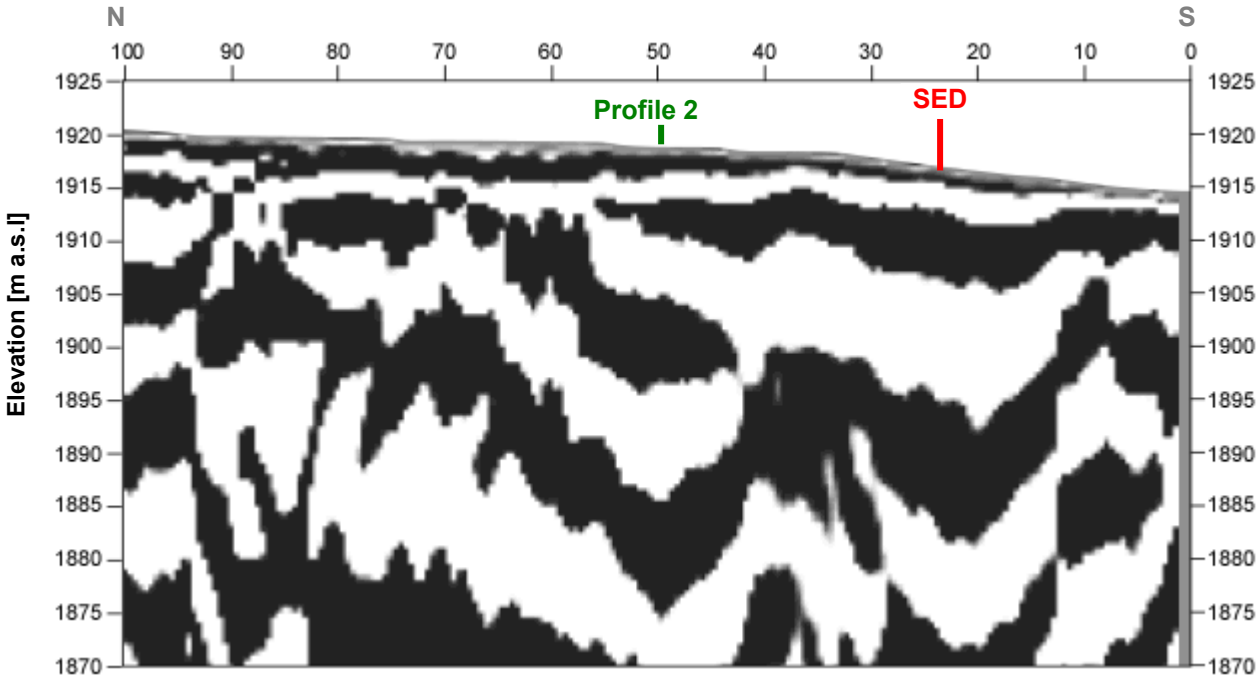

Fig. 3.4b: Seismic depth section of seismic line 09SN_11MUO-P1 with variable density mode presentation. Vertical axis: elevation [m a.s.l.], horizontal axis: profile meter; no vertical exaggeration. The station spacing is 1 m.

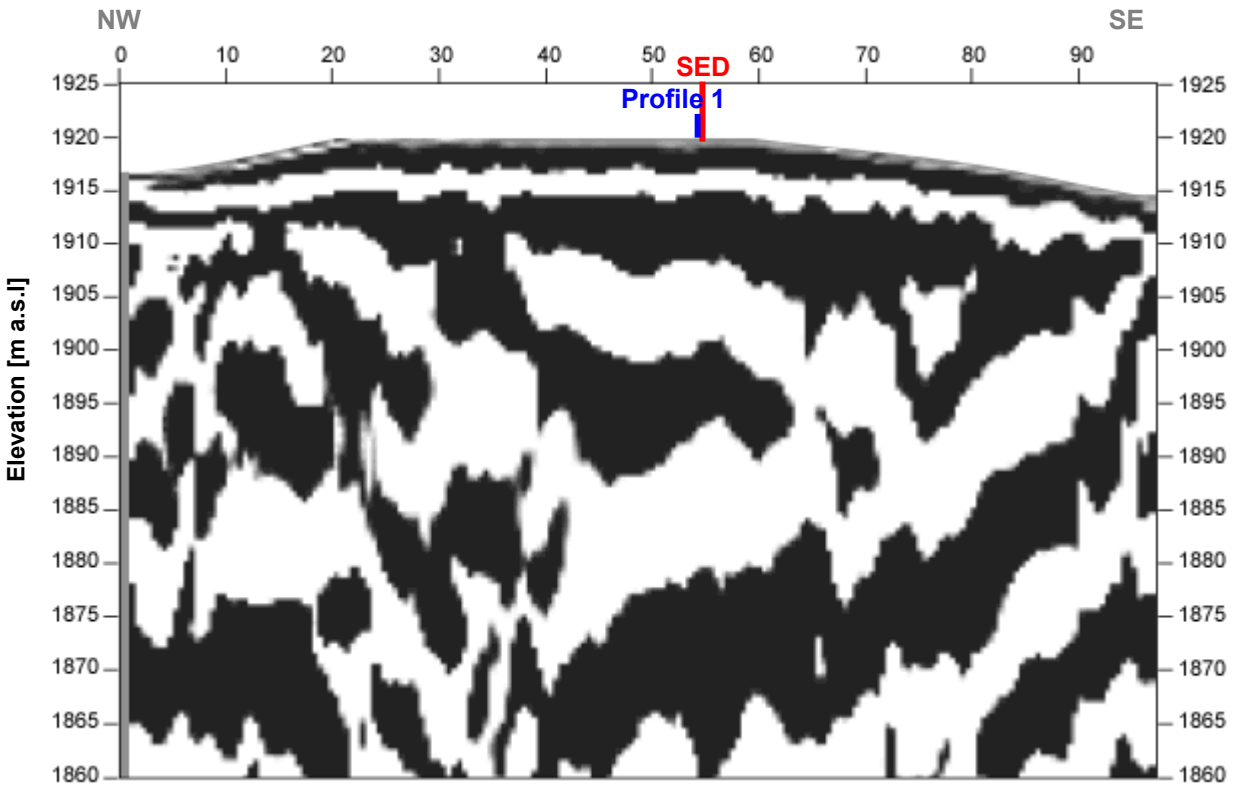

Fig. 3.4c: Seismic depth section of seismic line 09SN_111MUO-P1 with variable density mode presentation. Vertical axis: elevation [m a.s.l.], horizontal axis: profile meter; no vertical exaggeration. The station spacing is 1 m.

3.4.3 p-wave refraction tomography processing

The seismic p-wave refraction processing steps are analogous to those described in paragraph 3.2. For a detailed method statement and a description of the processing steps please refer to the summary report. The Figs. 3.4d to 3.4i and Tab. 3.4a illustrate the intermediate processing steps and the final result.

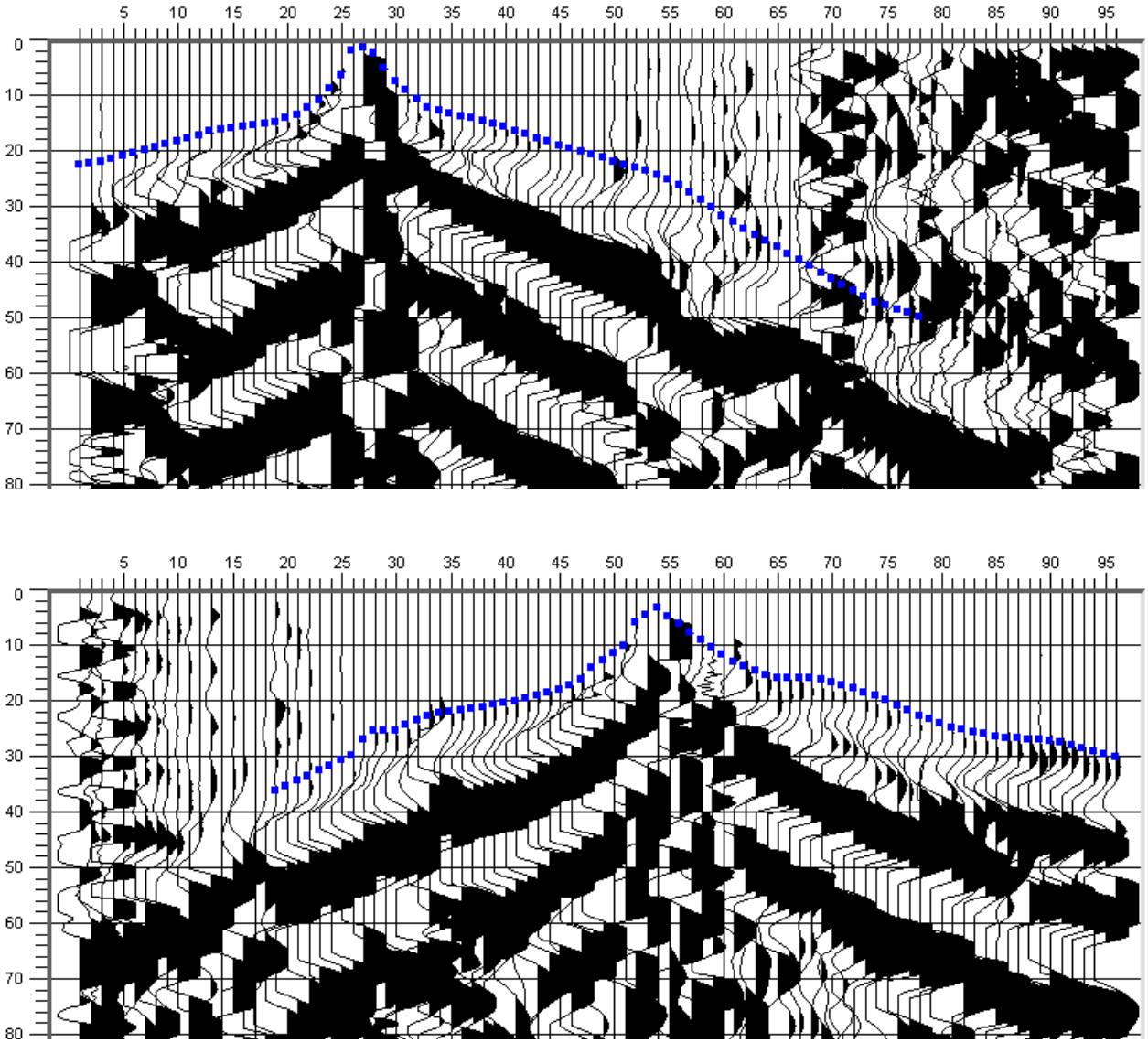

Fig. 3.4d: p-wave records of 09SN_11MUO-P1 (top) and -P2 (bottom) with positive amplitude excursions in black. Blue squares mark the manually picked first break arrival times. Vertical axis: travel time in ms, horizontal axis: station numbers spaced at 1 m.

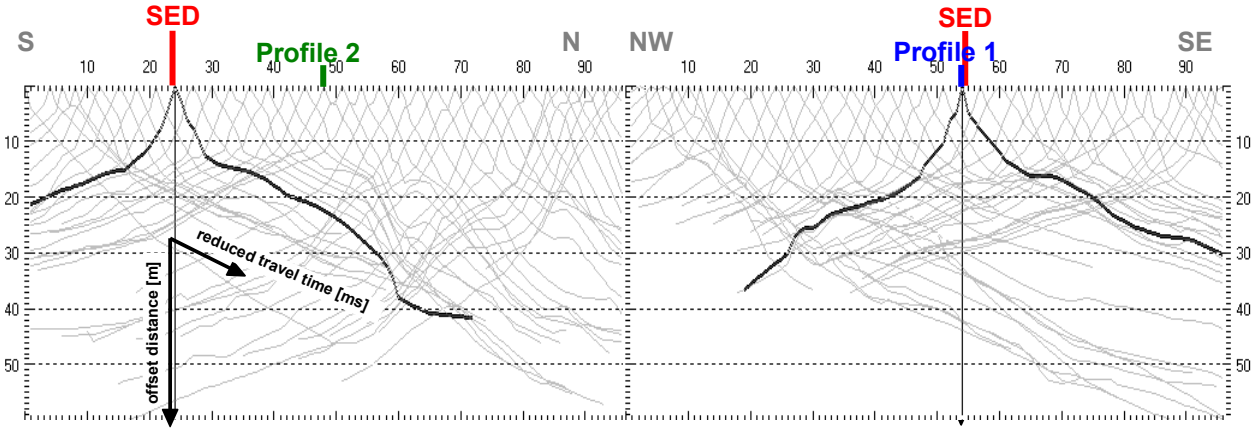

Fig. 3.4e: Travel time curves of p-wave arrival time picks of line 09SN_11MUO-P1 (left) and -P2 (right). Vertical axes: travel time [ms], horizontal axes: station number (= profile meter).

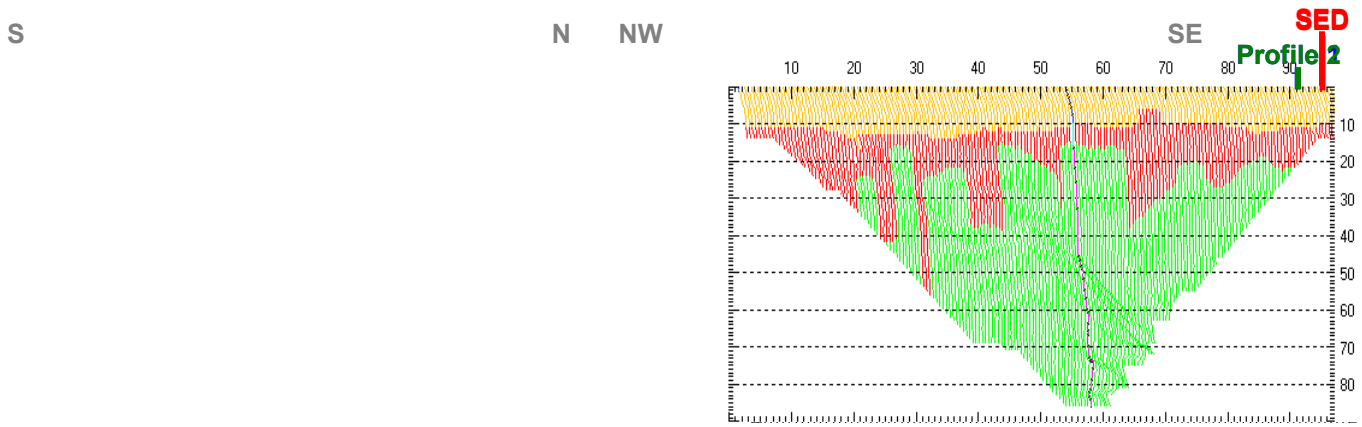

Fig. 3.4f: 3-dimensional distance-travel time diagrams at the mid-points between source points and receiver stations are instrumental when using the analytical CMP derivation of the initial velocity field. The horizontal axes are along the CMP positions and the travel time respectively, the vertical axis denotes the offset distance between source and receiver positions.

Depth [m]	Vp [m/s]
0.0	391
0.2	426
0.5	468
1.2	506
1.8	605
2.7	802
3.8	1168
5.2	1577
7.2	1586
9.8	1431
13.2	1634
17.8	2077
23.9	2672
32.0	2405

Depth [m]	Vp [m/s]
0.0	392
0.3	442
0.7	461
1.2	496
1.9	612
3.0	1014
4.4	1621
6.4	2290
9.3	2214
13.3	2384
18.9	2778
26.7	3242
37.7	3371
52.9	3358

Tab. 3.4a: Initial 1D p-wave velocity model derived from real data (left: 09SN_11MUO-P1; right: -P2).

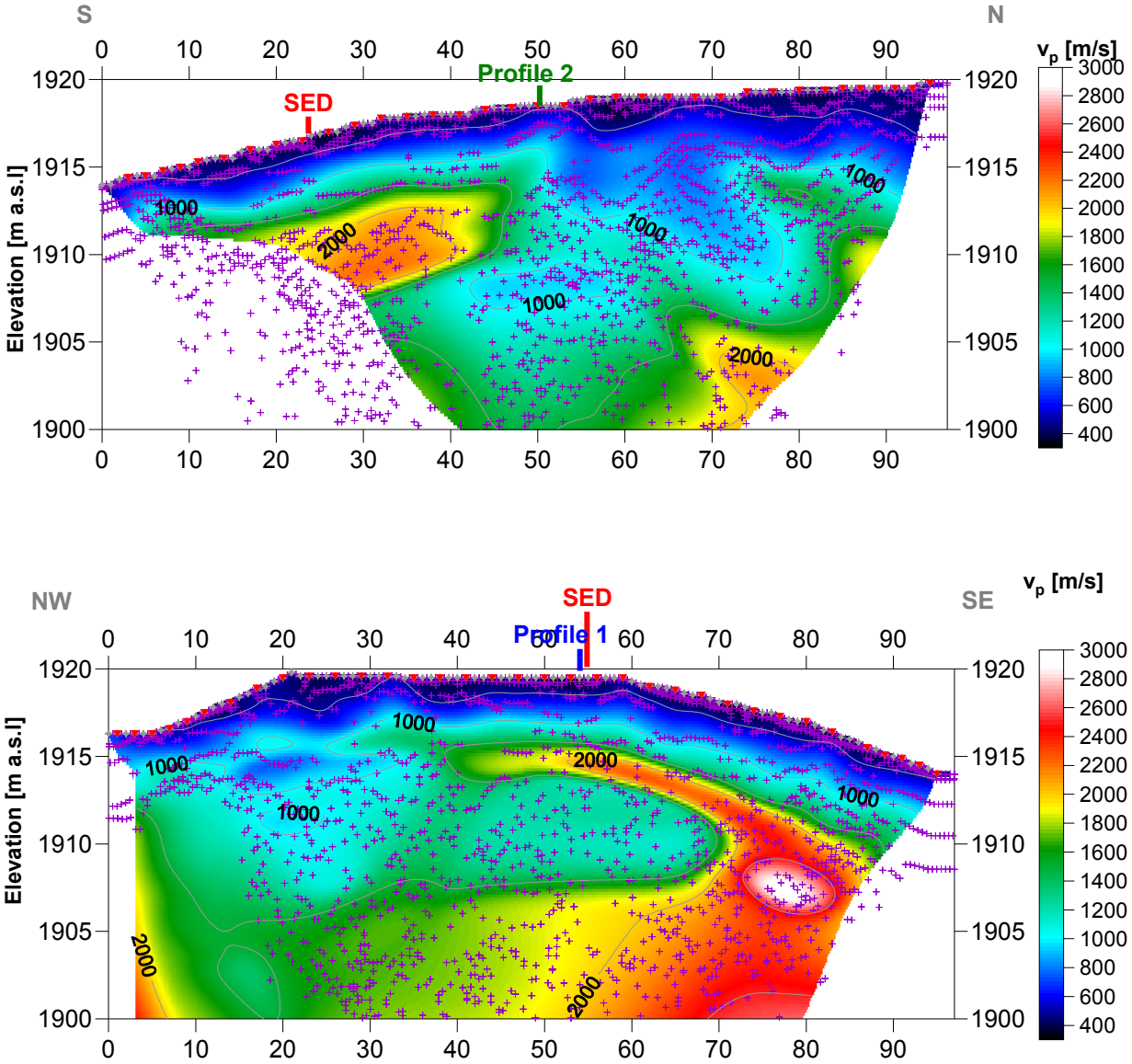

Fig. 3.4g: Compressional wave velocity field image along the seismic profiles 09SN-11MUO-P1 (top) and -P2 (bottom). Red/white colors indicate solid rock, blue/black colors unconsolidated sediments and soil. Vertical axis: elevation [m a.s.l]; horizontal axis: profile meter; color scale: v_S [m/s]; vertical exaggeration: 2:1; gray squares: receiver stations; red triangles: shot positions; magenta crosses: positions of determined velocity values.

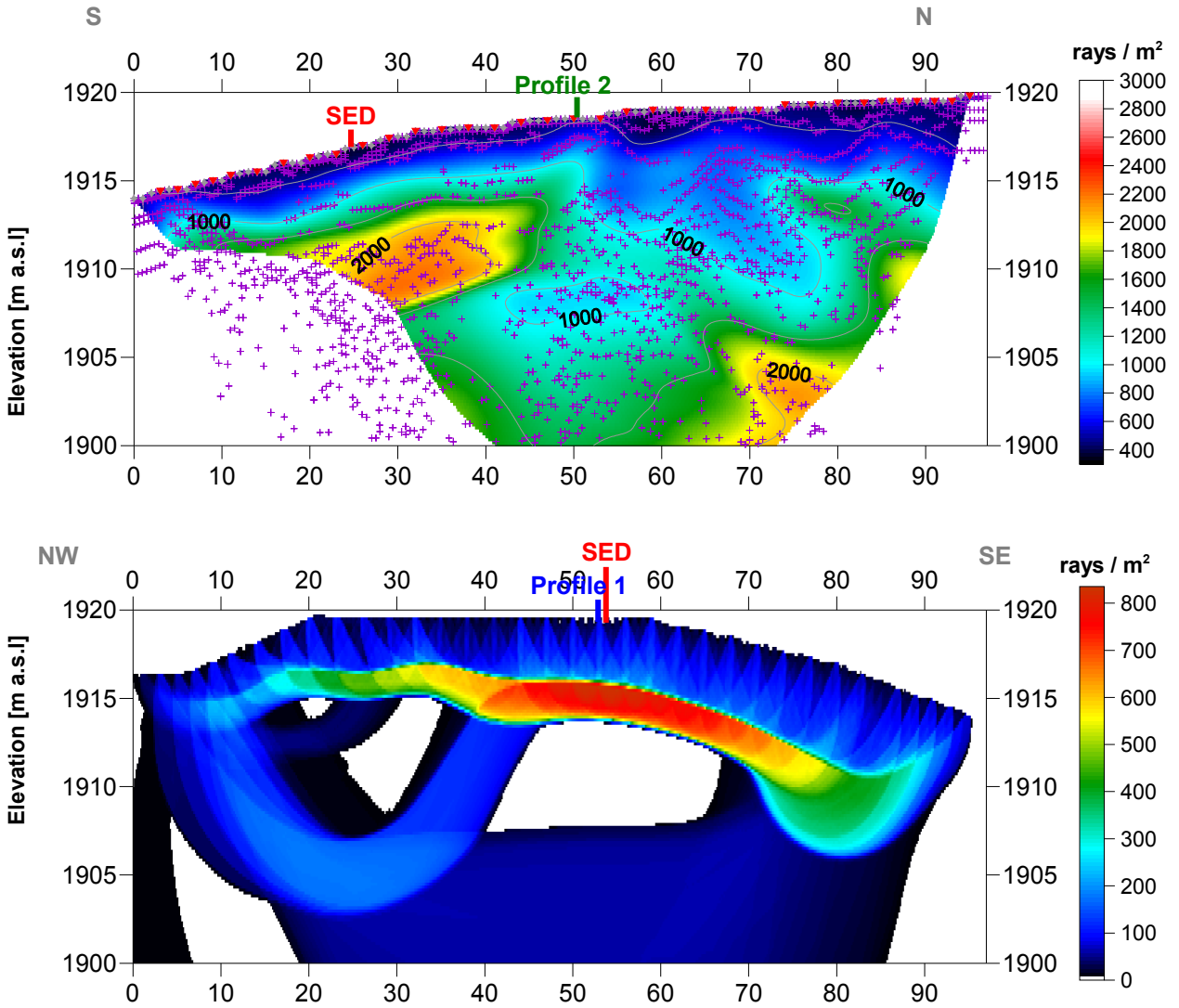

Fig. 3.4h Compressional wave subsurface ray path density along the seismic profiles 09SN_11MUO-P1 (above) and -P2 (below). Red/white colors indicate high velocity contrast between two layers, blue/black colors low coverage areas. Vertical axis: elevation [m a.s.l]; horizontal axis: profile meter; color scale: ray paths per m2; vertical exaggeration: 2:1.

Depth [m]	Vp [m/s]
0.0	432
1.5	604
2.8	895
4.2	1166
5.5	1386
6.8	1406
8.2	1421
9.5	1231
10.8	1165
12.2	1263
13.5	1433
14.8	1568
16.2	1624
17.5	1625
18.8	1673
20.2	1766
21.5	1843

Depth [m]	Vp [m/s]
0.0	412
2.2	813
4.4	1364
6.6	1438
8.8	1458
11.0	1572
13.2	1823
15.4	1903
17.6	1957
19.8	2036
22.0	2128
24.2	2222
26.4	2323
28.5	2424
30.7	2526
32.9	2585
35.1	2627
37.3	2719

Tab. 3.4b: Final 1D p-wave velocity model derived from real data at line 09SN_11MUO-P1 (left) resp. at line -P2 (right) .

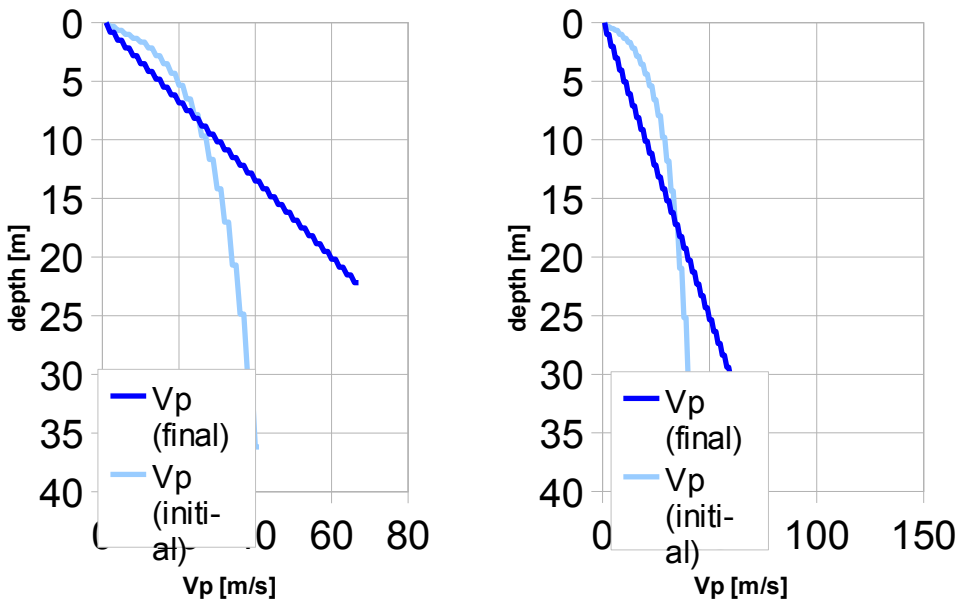

Fig. 3.4i: Final 1D p-wave velocity model derived from real data at line 09SN_11MUO-P1 (left) resp. at line -P2 (right). Initial 1D p-wave velocity model values are given in Tab. 3.4a.

3.4.4 Representation of the hybrid seismic section

The hybrid seismic section is the reflection seismic section with the superimposed p-wave velocity field. It portrays the geological structures and the p-wave velocity field, the latter being indicative for the rock / soil rigidity. The uninterpreted hybrid seismic section is portrayed in Fig. 3.4j and 3.4k below.

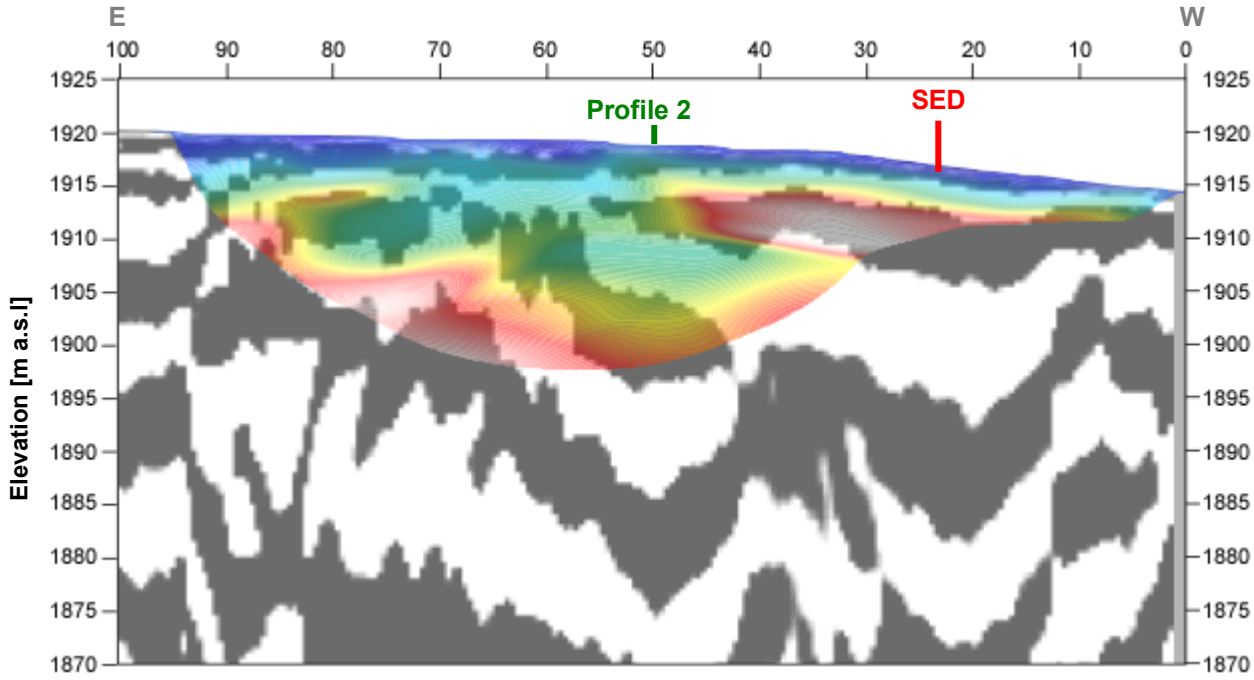

Fig. 3.4j Uninterpreted hybrid seismic section 09SN_11MUO-P1: superimposed onto the seismic reflection section is the color encoded p-velocity field derived by refraction tomography (no vertical exaggeration).

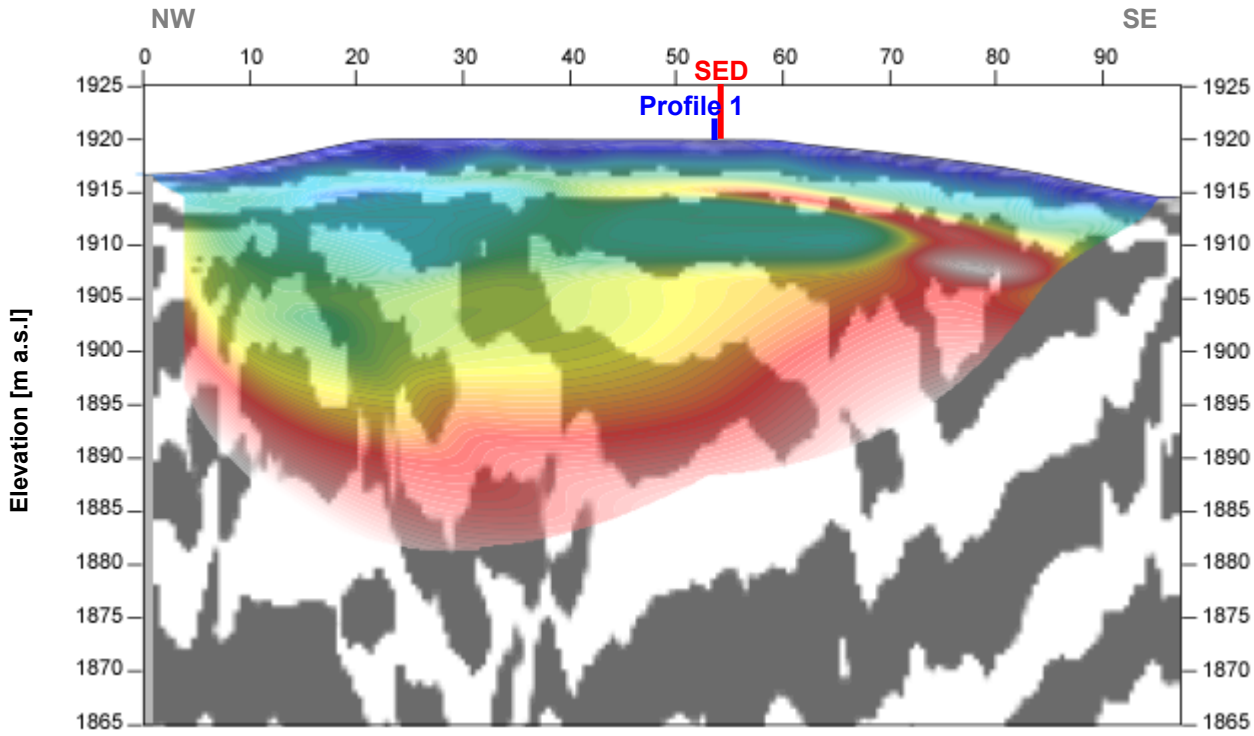

Fig. 3.4k Uninterpreted hybrid seismic section 09SN_11MUO-P2: superimposed onto the seismic reflection section is the color encoded p-velocity field derived by refraction tomography (no vertical exaggeration).

4 DISCUSSION OF THE RESULTS

4.1 Summary and Validation of the Results

Compressional and shear wave velocity data from refraction seismic surveys both p-wave and s-wave and also the MASW survey data of profiles 09SN_11MUO-1 and 09SN_11MUO-2 are shown in Tab. 4.1 for the uppermost 30 m. The calculated shear wave velocity $v_{s(calc)}$ in Tab. 4.1 is derived by using a theoretical v_p/v_s-ratio of $\sqrt{3}$.

Depth	Vp1	Vp2	Vs1	Vs1	Vs2	Vs2	Vs1	Vs2
	meas	meas	meas	calc	meas	calc	MASW	MASW
0.0	432	412	198	250	162	238	860	1105
1.0			400	0	352	0	884	1125
2.0	492	532	514	284	478	307	832	1116
3.0	742	768	665	429	595	443		
4.0	895	1050	708	517	778	606	776	1117
5.0	1166	1303	747	673	858	752		
6.0	1305	1486	773	754	992	858	771	1082
7.0	1406	1473	736	811	1031	850		
8.0	1406	1427	723	812	1053	824		1046
9.0	1421	1427	742	820	1064	824	862	
10.0	1346	1484	797	777	1050	857		
11.0	1158	1540	855	669	1055	889		
12.0	1165	1584	959	673	1065	914	1018	1109
13.0	1263	1706	930	729	1092	985		
14.0	1344	1823	1053	776	1111	1052		
15.0	1511	1876	1109	872	1148	1083		
16.0	1568	1898		905	1216	1096	1199	1320
17.0	1624	1919		938	1250	1108		
18.0	1616	1944		933	1304	1122		
19.0	1648	1985		951	1323	1146		
20.0	1673	2010		966	1353	1161		
21.0	1766	2063		1020	1372	1191	1288	1452
22.0	1806	2110		1043	1384	1218		
23.0		2149			1405	1241		
24.0		2190			1394	1264		
25.0		2233			1374	1289		
26.0		2277			1392	1314		
27.0		2323				1341	1553	1912
28.0		2363				1364		
29.0		2411				1392		
30.0		2461				1421		

Tab. 4.1: Shear and compressional wave velocity model determined at the SED station MUO.

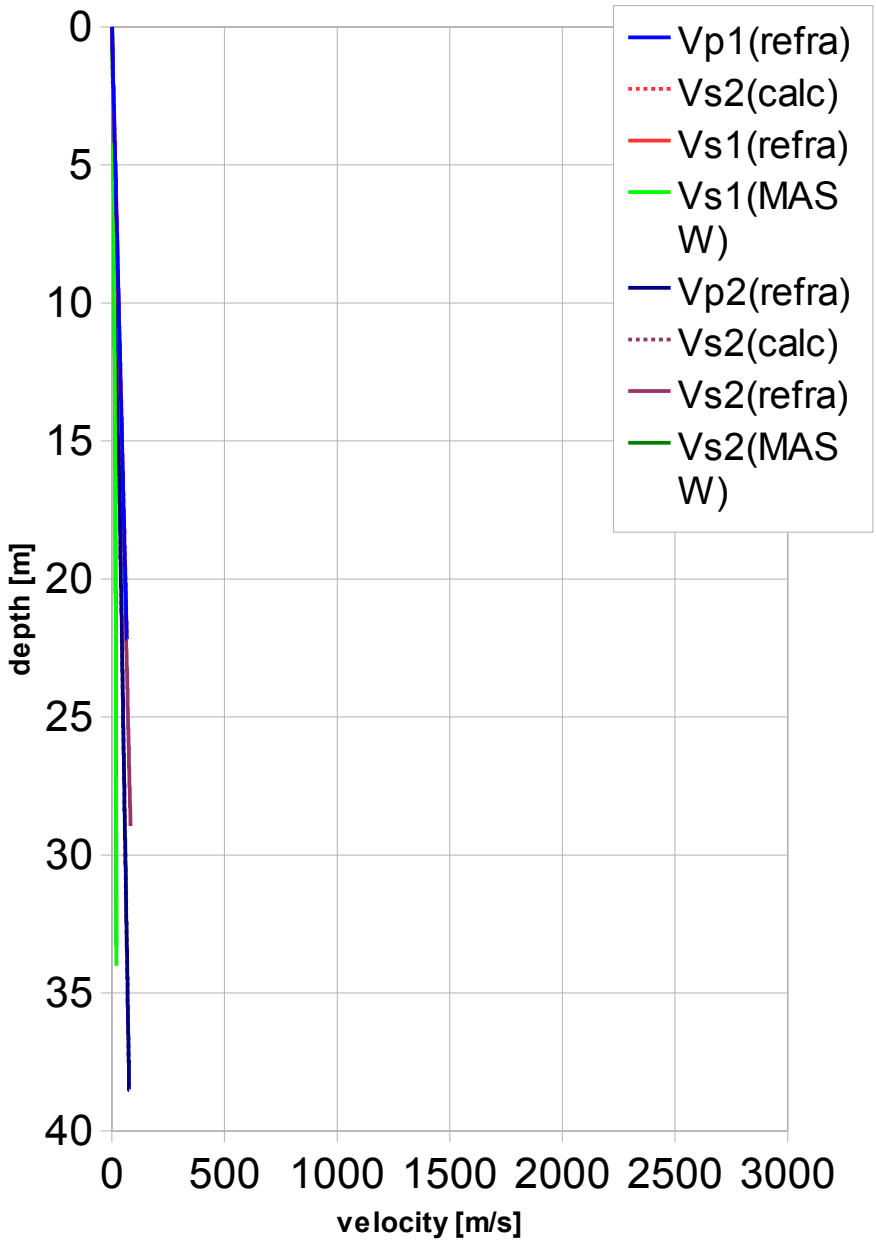

Fig. 4.1: Graphic display of shear (continuous lines) and compressional (dotted lines) wave velocities determined at the SED station. In green colors values of MASW analyses, in red values of shear wave refraction tomography and in blue of compressional refraction tomography. Dotted lines indicate maximal shear wave velocities derived by a theoretical v_p/v_s-ratio of $\sqrt{3}$.

4.2 Validation of the methods and their results

Due to methodological differences, v_s velocities derived by MASW analysis and by the refraction tomography technique may differ considerably. This is because MASW analysis cannot image small rock/soil inhomogeneities as a dispersion image with an array length of i.e. 40-m only yields one single v_s-value at each depth. On the other hand, refraction diving wave tomography results produce v_s-sections with a high lateral resolution, but fail to provide information at greater depths.

4.3 Error Estimates

The error estimates given in Tab. 4.3 below are relevant only in the context of this survey.

Surveying method	Type of result	Error estimate
v_s – refraction tomography	v_s – velocity field image	10%
MASW only "+" or only "-" values*	v_s – velocity field image	15%
MASW (mean of "+" & "-" values)*	v_s – velocity field image	10%
v_p – refraction tomography	v_p – velocity field image	8%
Reflection seismic surveying	Image of subsurface structures	n.a.

** MASW values in the uppermost 6 m are prone to an error of about 30 % (only one direction) resp. 20 % (mean of both directions.*

Tab. 4.3 Error estimates for the methods applied. Note that higher error estimates are to be taken into account with increasing depths.

The above error estimates are of a qualitative character only. In view of the intense fluctuations to be expected in both the lateral and vertical directions, any attempt to derive a quantitative general error estimate to be valid for the entire survey is to be considered as futile. In particular possibly existing military bunkers and galleries below the survey site (in which the earthquake monitoring station is positioned) on both seismic lines have a certain impact on the quality of dispersion images. Nevertheless, all velocity data coincide well, independently of the methodological differences.

In the uppermost ~6 m, the MASW derived shear wave velocities are considerably higher than the refraction tomography values. In greater depths, they correspond well.

4.4 The Geophysical Interpretation

The most conclusive information about the subsurface structures is provided by the results of the hybrid seismic section (v_p-refraction tomography profiling and reflection seismic section) and confirmed by the evaluation results of the v_s-refraction tomography data.

As can be seen from the v_s and v_p refraction tomography sections in Fig. 3.2e/f & Fig. 3.4g/h, the topography of the bedrock surface is vaguely imaged on both profiles. The geological interpretation of the seismic events is shown in Fig. 4.2a. The rock surface is found not deeper than in 4 m depth. To the South, the bedrock surface is situated nearest to terrain and in the North in a depth of 4 m. Between profile meter 50 and 70, the hard rock surface seems to be broken and possibly it deepens to a depth of 5 to 7 m.

The bedrocks layering is characterized by folds, disturbed by tectonic faults. The velocity field may image the military galleries.

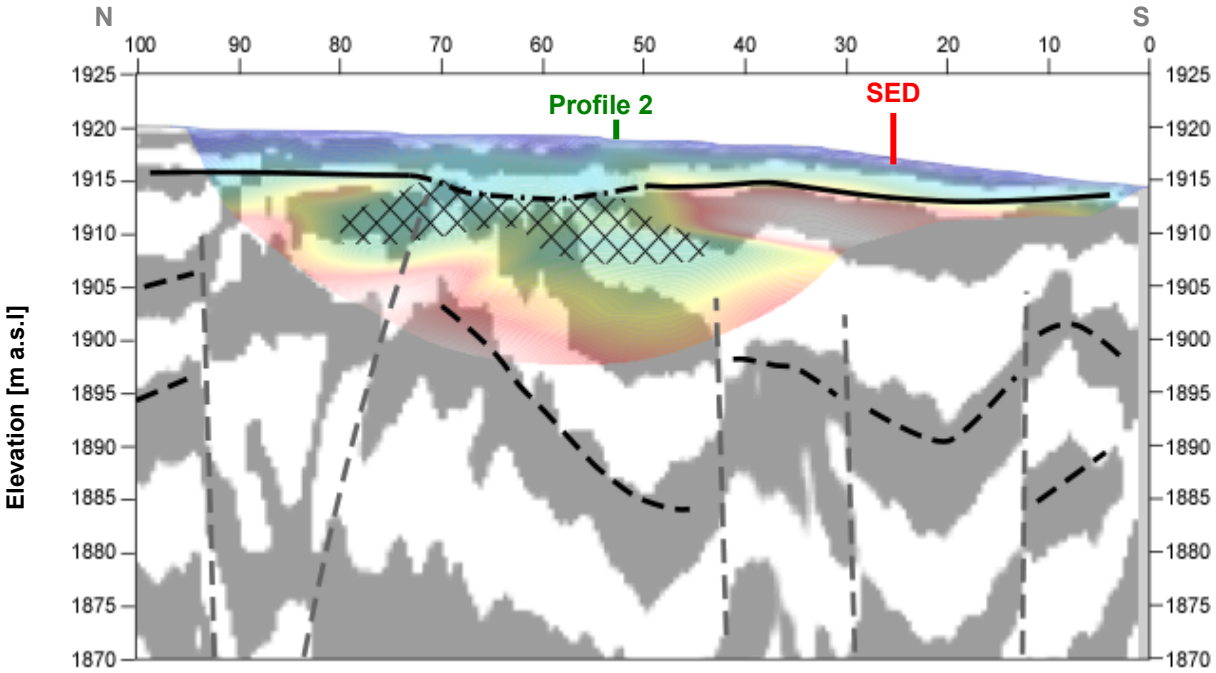

Fig. 4.2a Geophysical interpretation of the hybrid seismic section 09SN_11MUO-P1. Black lines denote layer boundaries, the continuous one – and between profile meter 50 and 70 with a chain dotted line the uncertainty – the bedrock surface. Gray steep dashed lines image tectonic faults. The hatched area visualizes the reduced velocities zone.

The geological interpretation of the seismic events of line 09SN_11MUO-2 is shown in Fig. 4.2a. The topography of the bedrock surface is imaged in detail in the SE part of the profile, vaguely in the NW part. The bedrock surface is found all over the profile in less than 5 m. As in profile 09SN_11MUO-1, a reduced velocity zone is given in the NW part. Two tectonic faults disturb the bedrocks folded layering.

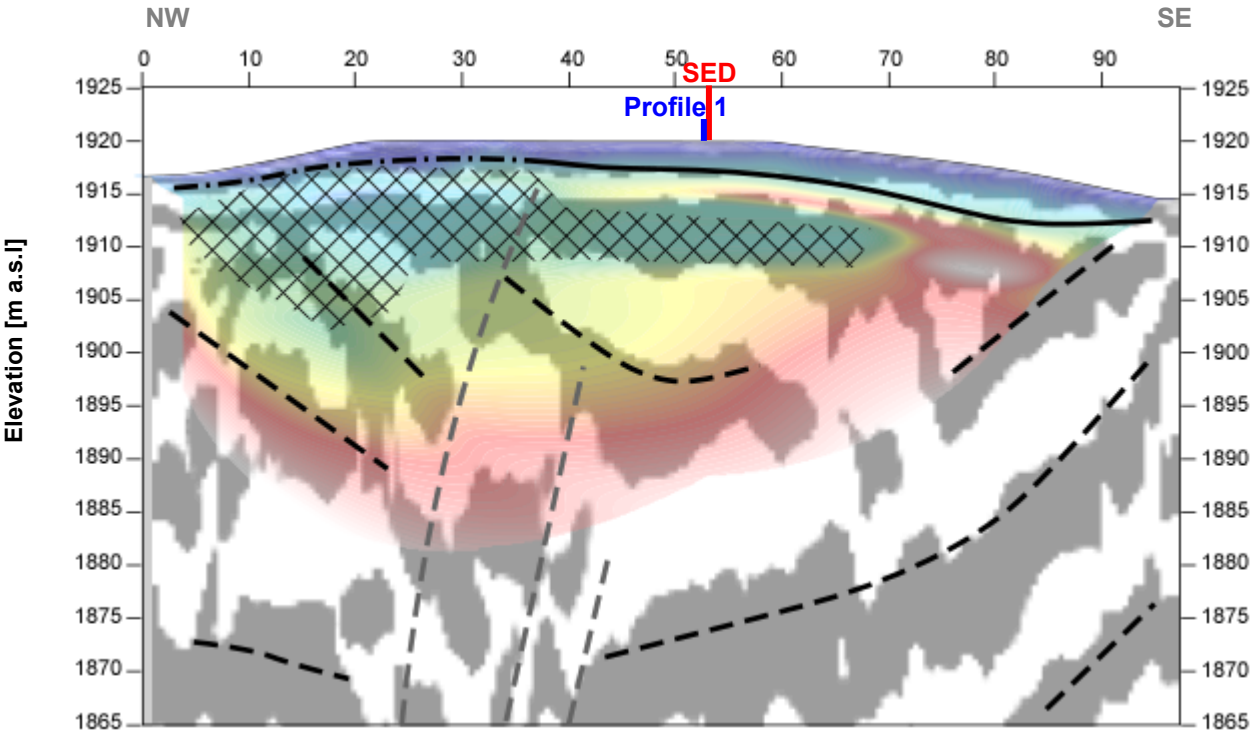

Fig. 4.2b Geophysical interpretation of the hybrid seismic section 09SN_11MUO-P2. Black lines denote layer boundaries, the continuous one – and between profile meter 50 and 70 with a chain dotted line the uncertainty – the bedrock surface. Gray steep dashed lines image tectonic faults. The hatched area visualizes the reduced velocities zone.

5 SUMMARY AND CONCLUSIONS

- In June 2009 a combined seismic s- and p-wave survey was carried out at the SED earthquake monitoring station MUO near Morschach SZ.
- The shear wave data have been evaluated by conventional diving wave refraction tomography techniques in order to derive the s-wave velocity field along the seismic line.
- The p-wave data have been processed

• firstly to derive a 2D s-wave velocity field by using the MASW (**M**ultichannel **A**nalysis of **S**urface **W**aves) technique;

• and secondly, according to the hybrid seismic data processing scheme for representing the subsurface structures in a combined reflection seismic section with the superimposed p-wave velocity field.

- The shear wave velocity range determined by the MASW method in the uppermost 30 meters spans from values of 771 m/s to 1912 m/s.
- The scalar values derived by the MASW survey at the SED station (seismic line 09SN_11MUO-M1 resp. line 09SN_11MUO-M2) are the following:

line 1			line 2		
$v_{s,5}$	=	862 m/s	$v_{s,5}$	=	1129 m/s
$v_{s,10}$	=	809 m/s	$v_{s,10}$	=	1113 m/s
$v_{s,20}$	=	877 m/s	$v_{s,20}$	=	1111 m/s
$v_{s,30}$	=	970 m/s	$v_{s,30}$	=	1179 m/s
$v_{s,40}$	=	n/a	$v_{s,40}$	=	n/a

- The estimated reliable refraction shear wave velocity derived is 1100 m/s.
- The estimated reliable refraction compressional wave velocity derived is 2000 m/s.
- The geophysical interpretation of the subsurface structures in this report are to be validated and incorporated into a comprehensive appraisal by a geologist familiar with the local geological setting.

Schwerzenbach, 13th July 2009

Walter Frei
dipl. Natw. ETH
managing director

Lorenz Keller
dipl. Natw. ETH
project manager